Tampere University

FETSUME BERHE

IMAGE TEXTURE ANALYSIS FOR PROSTATE CANCER DETECTION

Faculty of medicine and health technology
Master's thesis
May 2019

ABSTRACT

Fetsume Berhe: image texture analysis for prostate cancer detection
Master's thesis
Tampere University
Biomedical engineering
May 2019

Recent advancement in diagnostic imaging has made the mortality rate associated with prostate cancer (PCa) to decrease drastically. Given to lower threshold cut-off values for prostate-specific antigen (PSA) which is the primary augury aside from clinical signs and symptoms for the presence of cancer and indication for ultrasound-guided biopsy analysis. Due to its availability, low cost, justification and well tolerance of the patient, ultrasound (US) stays to be the golden modality for prostate evaluation and real-time biopsy guidance.

While US stays to be in the first line of a diagnostic prediction method for the presence of PCa it is mainly used for biopsy guidance on account of its lower sensitivity and specificity towards the differential of cancer from other pathologies and relatively high rate of false negative results.

Due to the variable sonographic appearance of the malignancy and its similarity with the non-malignant conditions, it is always possible only to differentiate cancer from the non-cancerous conditions by using biopsy. Moreover, in cases where malignant conditions are apparent together with the non-malignant pathologies there will be the superimposition of echo signals making the differential diagnosis difficult.

Image processing and texture analysis can improve the diagnostic details obtained from digital diagnostic two-dimensional (2D) or three-dimensional (3D) images. We can analyze the image texture parameters quantitatively using the specific MaZda software to ascertain different anatomy for distinguishing normal from the abnormal tissue structures.

In this thesis work prostate, US images texture parameters are analyzed using MaZda software to distinguish the classic texture distribution of PCa. All patients in the study had elevated PSA value and biopsy has confirmed the presence of malignancy.

Keywords: ultrasound, prostate cancer, sensitivity, specificity, pixel, voxel, image processing, texture, texture analysis, MaZda, region of interest (ROI)

PREFACE

This Master of Science thesis major in medical physics is carried out in Tampere university hospital in the department of radiology, Tampere University, Tampere, Finland.

First and above all I would like to give salute to JESUS! For taking me through those unimaginable and unexplainable years of my life and help me to focus and strengthen me while I was doing this thesis work. And I would like to greatly thank my supervisor professor Hannu Eskola for giving me this opportunity to work on the subject that I am most interested and for his time, kind guidance and appreciation while I was doing the work.

I would also like to thank Dr.Antti Kaipia for giving me this opportunity to work in his department, allowing all the the necessary material inputs to be used for this thesis work and for facilitating the practical demonstration in the urology department when needed.

I would also like to thank Dr. Anna Vuorenmaa for helping me by giving clear instructions and the means to download MaZda and by preparing the ultrasound images to be suited to use it in the software. I was also getting a real help from Dr. Anna by phone message whenever there is a new instruction or updates on any stage of the thesis writing processes. She was also very kind and highly responsive for all my emails whenever I was facing problems with the images or the software.

Fetsume Berhe Kiros.

ፍጹም በርሔ(ወዲ ኪሮስ)

April 2019

CONTENTS

LIST OF SYMBOLS AND ABBREVIATIONS

2D	Two-dimensional
3D	Three-dimensional
AFMS	Anterior fibromuscular stroma
AR	Androgen receptor
BPH	Benign prostatic hyperplasia
C	Speed
COM	Co-occurrence matrix
CZ	Central zone
DHT	Dihydrotestestrone
DRE	Digital rectal examination
ED	Ejaculatory duct
FDA	Food and drug administration
MRI	Magnetic resonance imaging
MaZda	“Maceierz Zdarzen”
PA	Prostate artery
PAE	Prostate artery embolization
PCa	Prostate cancer
PIA	Proliferative inflammatory atrophy
PIN	Prostate intraepithelial Neoplasm
PSA	Prostate specific antigen
PSAD	Prostate specific antigen density
PSAV	Prostate specific antigen velocity
PZ	Peripheral zone
RLM	Run-length matrix
ROI	Region of interest
SVs	Seminal vesicles
TRUS	Trans-rectal ultrasound
TZ	Transition zone
UB	Urinary bladder
US	Ultrasound
Z	Acoustic impedance
f	Frequency

1. INTRODUCTION

Complications related to prostate are most prevalent in men with age beginning from 30 years. Most men who are diagnosed with prostate pathologies are in their mid or above mid ages. The most common disease associated with the gland is benign prostatic hyperplasia (BPH) which is the benign enlargement of the prostate tissue with no associated malignant cell proliferation and angiogenesis, PCa is the cancerous proliferation of the cells and there is a possibility of infiltrating to the surrounding structures. prostatitis (acute and chronic) is the inflammatory reaction of prostate towards bacterial or viral invasion and antibiotics can be prescribed to alleviate the problem, calcifications are the presence of smaller stones in the gland and they can be caused secondary to ongoing pathologies such as BPH and PCa [1].

The major focus of this thesis work is on PCa pathophysiology, routine clinical and radiological diagnostic methods and the most recent advancement in medical image processing and image texture analysis using MaZda that improves the diagnostic information obtained from the digital diagnostic 2 D or 3D images.

PCa is the most common malignancy (adenocarcinoma in 95% of cases) in men and the second leading cause of mortality in the US [2]. As per the American cancer society statistics, 180,890 new cases are observed each year and in 2016 only the death rate was recorded at 26,120[1].

The etiology of the disease is not known but the epidemiology has a big variation based on the difference in age, ethnic class, geographical location, family hereditary history and the way of lifestyle. It is predicted that the incidence of the disease will increase in the future especially in western and other developed nations due to the higher proportion of the aging population. In general, the probability of being diagnosed with PCa throughout the person's lifetime is 11% and 1 in 26 dies from the confirmed malignancy and its complications [3].

Early detection of PCa is the crucial step for the availability of a wide range of treatment options to be chosen, increased patient comfort towards the treatment, better treatment response and higher survival rate. Screening programs mainly targeting those who are above 50 years of age and with a positive family hereditary history has made the mortality

rate drastically low [4]. Blood test to evaluate if there is an elevated level of PSA, a glycoprotein secreted by prostate in normal conditions, which does liquefy the seminal fluid in order to improve the motility of the sperm and act as a basic buffer to neutralize the acidic vaginal and cervical environment, is a precursor to suspect the presence of PCa. The major drawback of the screening option using PSA assessment is that it has a higher rate of false positive and false negative results. It has been observed that a PSA level above 4µg/L has a 37% sensitivity to malignancy and 15% of those who have PSA level less than 4ng/L has shown adenocarcinoma during a biopsy. This is because the amount of the protein (PSA) secretion may be increased related to other pathologies other than PCa and at a normal situation the PSA serum level is increased in direct proportion with age, this has made the interpretation ambiguous and the result has to be always compared with the medical history of the patient. PSA evaluation can be combined with Digital rectal examination (DRE) which enables the clinician to assess the structure of prostate by palpitation in order to affirm if there is any tissue irregularity is also another screening option [5, 6].

Trans-rectal ultrasound (TRUS) is the major imaging modality that can be used if the patient has no any contraindication such as prostatitis, Crohn's disease and no abdominoperineal resection for imaging of prostate to detect PCa. 70% of the adenocarcinoma is originating from the peripheral zone (PZ). At normal condition, the PZ has a higher echo signal than the CZ and TZ. Any abnormality in echo signal, boundary irregularity, the presence of nodular foci and angiogenesis in this zone is a strong indication of malignant invasion. Most of the time the ultrasonic appearance of PCa is hypoechoic but it can vary from hyperechoic mimicking BPH to isoechoic as in prostatitis. Although TRUS is the widely accepted diagnostic method it has a low sensitivity and specificity with 50-60 % accuracy. This is the major reason biopsy using TRUS guidance has to be taken and confirmand [6].

The lack of sensitivity and specificity is the main limitation in the current diagnostic methods in use. Increasing the diagnostic information obtained from the medical digital 2D or 3D images using image texture analysis can increase the diagnostic accuracy and avoid unnecessary repeat procedures that will decrease the economic expenses and increase patient comfort avoiding invasive procedures.

MaZda is a software package developed by European COST B11 project, the intention of the project was to develop a method for mathematical texture analysis of MRI images. The name of the software MaZda emerges from the texture parameter that was primarily analyzed (co-occurrence matrix, that is based on statistical distributions of image textures) which is spelled “Maceierz Zdarzen” in polish language. MaZda gives a free choice

to use the whole image or choose a specific region of interest (ROI) to be further analyzed. The results of the analysis can be presented in the form of image feature distribution (feature maps) or in the form of a text list of the features (feature vectors) which is subjective to choice [7, 8].

2. THEORETICAL BACKGROUND

2.1 Prostate anatomy

Prostate belongs to the male accessory reproductive organs, which secretes a basic fluid. The organ is composed of both glandular and stromal components adjoined by a fibrous capsule with inner smooth muscle and outer collagen layers [9].

The name prostate comes from the Greek word “prohistani” meaning to stand in front. The prostate got its name from its regional anatomic position, which it stands in front of the urinary bladder. The fluid-filled urinary bladder (UB) is used as a diagnostic window to measure prostate volume for diagnosis of prostate pathologies using transabdominal ultrasound. An abnormal volume might be an indication of disease prognosis such as BPH and PCa [10].

Regionally prostate is located in the subperitoneal space below the pelvic diaphragm bordered by the symphysis pubis anteriorly, rectum posteriorly and the UB superiorly. In non-pathologic condition, the gland measures 4 cm in transverse, 3cm in vertical and 2cm in anteroposterior directions with a total weight of approximately 18g. In a normal adult, the gland has a walnut shape with ventral, dorsal and lateral surfaces. While the superior broader surface of the prostate (base) is continuous with the apex of the UB the inferior narrower surface (apex) rests on the urogenital diaphragm [2, 9, 11]. The lateral pelvic wall makes a border with the two inferolateral apical surfaces bilaterally. The pre-prostatic urethra enters the prostate traversing the base at mid-section and becomes prostatic urethra and exit later from the anterior surface close to the apex, while the ejaculatory ducts enter into the gland from the posterior surface of the base and terminate at the verumontanum. The posterior aspect of the prostate and seminal vesicles are separated from the rectum by the thin layer of connective tissues called the denonvillier’s fascia, which is used as a surgical excision border for rectal cancer [12]. Figure 2.1.1 shows the regional relation of prostate within the pelvic cavity.

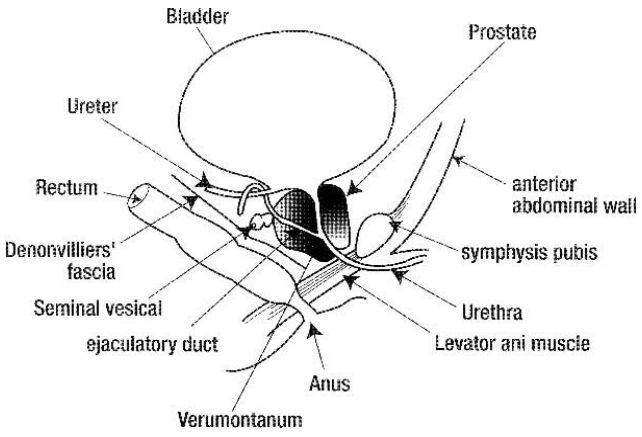

Figure 2.1.1 *Cross-sectional anatomy of male pelvis showing the regional relation of the Prostate with the surrounding structures [13].*

Initially, the lobar concept of prostate anatomic classification that was based on similarity with an animal was widely in use. However, due to lack of distinct lobes in humans, it was later replaced by MacNeal zonal division system [12]. Accordingly, the prostate is divided into four distinct zones based on histologic, anatomical (structural) and rate of pathologic incidences. The central zone (CZ), transition zone (TZ) and the peripheral zone (PZ) comprise the glandular section of the prostate (that constitute 70% of the total volume of the gland) while the anterior fibromuscular stroma (AFMS) belongs to the muscular component (compose 30 % of the total prostate volume) [9, 11, 14].

PZ is the largest of all zonal compartments covering 70% of the prostate glandular tissues. It encompasses the dorsal, apical and inferior section of the prostate. The secretory ducts in this zone are emptied directly to the prostatic urethra in its entire length. This is the typical zone for the manifestation of PCa and chronic infections (prostatitis) [9].

The CZ which is enclosed in between PZ and TZ comprise 25% of the prostate glandular tissue mainly forms the base of the prostate. It has a cone shape morphology where the apex terminates at the verumontanum (V). The ejaculatory ducts (ED) traverse this section to meet the prostatic urethra at the V [9]. This zone is less likely to be infiltrated with malignancy and only 1-5% of PCa emanates from this zone [11]. CZ will undergo atrophic change associated with aging and hypertrophy of the TZ (BPH) will have a mass effect on this zone [12]. The ductal tract from this zone follows the path of the ED to be inserted at the V [15, 14].

TZ constitute 5% of the glandular tissues surrounding bilaterally the mid part of the prostatic urethra. This zone is the main susceptible section for BPH with a mass effect (compress) on the urethra that will be presented as symptoms related to UB obstruction [9, 14].The ventral section of the prostate is enclosed by the AFMS that doesn't have any glandular tissue but muscular tissue. The distal section of this zone is important as a constriction function to eject secretory products [15]. Figure 2.1.2 shows the glandular and stromal area of prostate and their interrelationship.

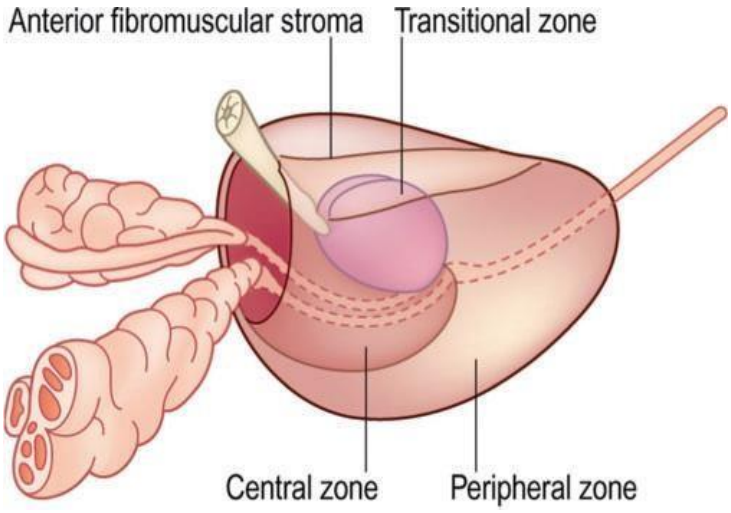

***Figure 2.1.2**. Zonal classification of a Prostate. The TZ surrounds the Prostatic urethra bilaterally near the V. CZ is traversed by the ED. The PZ enclose both the CZ and PZ except the anterior surface where AFMS is located [3].*

The bilateral neurovascular bundles are located in the posterolateral aspect of the gland and it regulates the structural development, function, and specialization of the prostate cells. This site also affects sexual activity such as penile erections. Any medical management procedure for prostate treatment has to avoid the occurrence of any complication on this site [12]. It is also the primary area of interest for contrast and Anastasia administration during contrast-enhanced Doppler ultrasound and during TRUS guided biopsy extraction. Disease prognosis especially PCa can be evaluated by assessing this area for any irregularity and angiogenesis since the lymphatic and the vascular plexus are the primary route for adenocarcinomas metastasis [3, 12].

Seminal vesicles (SVs) located cephalic to the base of the prostate join the vas deferens (VD) bilaterally to form the ED that is inserted to the urethra at the V. It is rare that the SVs become the primary site for any of the prostate pathologies but their inspection is vital in order to asses if there is advanced PCa [12].

The vascular supply to the prostate may originate from different sources in different individuals and it is observed that there is a variation in the number of branches between the right and left side of the gland. The prostatic artery (PA) may originate from either the anterior gluteal–pudendal trunk, obturator artery, internal pudendal artery or inferior gluteal artery. The arterial supply to the prostate will branch from one of the origins mentioned as a prostate-visceral artery and later re-branch into inferior visceral artery and PA to supply the gland. Identifying the correct branching and direction of the PAs is very important during prostate artery embolization (PAE) for the treatment of BPH. Correct catheterization of PA before PAE will avoid ischemic complications to the surrounding organs including the bladder by avoiding unwanted embolization of arteries supplying the organs other than the prostate [16]. Figure 2.1.3 illustrates the possible origins of vascular supply to prostate in different individuals.

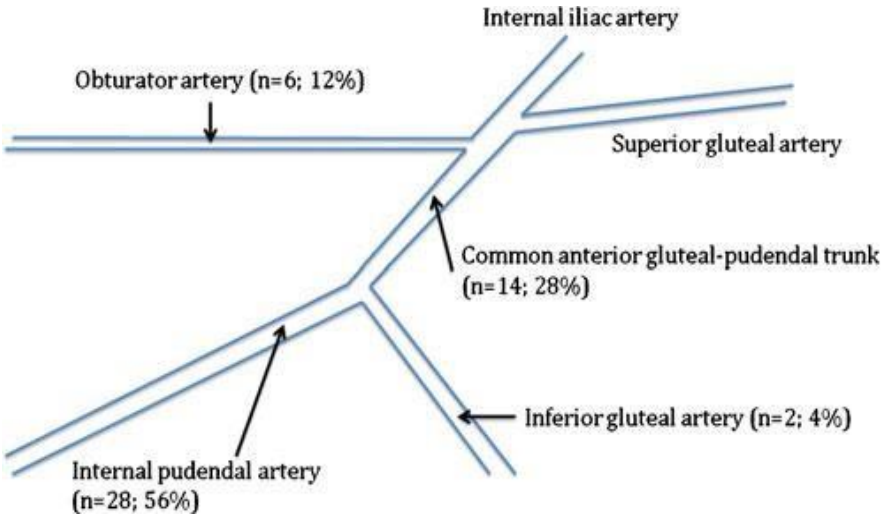

Figure 2.1.3 *Possible origin of PA, the internal iliac artery is the source of all the possible origins of the PA. The internal pudental artery is the most common origin for PA. The result was found by studying 25 (n=25) cadaveric specimens with 2x25(50) male pelvic side in total and associated percentage of samples with the same PA origin [16].*

2.2 Prostate physiology

The prostate is composed of 30-50 branching tubules that terminate in secretary alveoli and a stroma, which is mainly muscular. Both the glandular and muscular components are covered by a fibrous capsule that separates the gland into compartments of lobules. The glandular tissue is arranged in the three layers, mucosa, submucosa and upper layer from inner to an outer surface. The outer surface is the main surface that contains most

of the secretory cells. The prostatic ducts from the inner glandular layer directly open into the prostatic urethra and the ducts from the rest of the glandular tissues are attached with the prostatic sinus on the ventral aspect of the urethra. The secretory products are forced into the urethra by using the involuntary contraction of the FMS [17].

The glandular epithelium is composed of secretory cells (SCs), basal cells (BCs), stem cells, amplifying cells and neuroendocrine cells. Luminal cells or SCs are the most abundant type of cells. prostate-specific antigen (PSA) and prostate acid phosphate (PAP) are the major secretory products of these cells. They are dependent on androgen (cytokeratins 8 and 18 are cell surface androgen receptors) for their function, proliferation, and differentiation [17].

Stem cells are located close to the basement membrane and they have a capability of differentiating to secretory cells. They can undergo both symmetric and asymmetric division in order to self-renew or specialize to become luminal cells (SCs) of the prostate epithelium. Asymmetric cell division of stem cells will result in a production of two daughter cells one with identical with the parent steam cell to replenish themselves and progenitor cells that will later specialize to intermediate cells, the intermediate cells will again differentiate to become SCs and neuroendocrine cells [17]. Figure 2.2.1 illustrates the cellular architecture of prostate tissues.

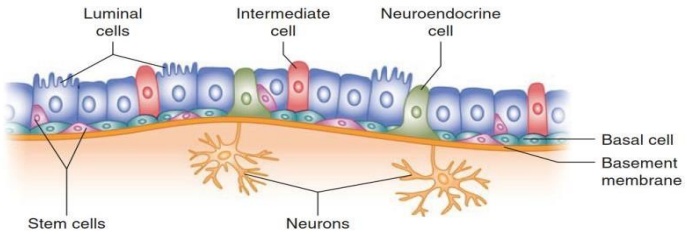

Figure 2.2.1 *The cellular anatomy of prostate epithelium. The stem cells have a capability of both self-renewal and differentiate into either BCs or SCs. the intermediate cells have the same cell markers as the SCs and BCs [18].*

Neuroendocrine cells (NECs) are highly differentiated cell types which are contained all over the lumen and some of them (open types) has longer branches that extend to be in contact with the lumen and the second types (open) does not have any extension towards the lumen. They are independent of androgen and chromogranin is their cell surface marker. They have a monitoring function on the development, specialization and physiologic balance of the glandular function [17].

2.3 Prostate cancer (PCa)

PCa can either originate from tumors that are derived from the glandular epithelial section or from the muscular tissue component. Tumors originating from the secretory component of the gland has different structural emergence that will be the base for their classification, the majority of them (90%) have an acinar appearance with microacinar, atrophic, Pseudohyperplastic and signet ring as their sub-types [19]. Almost 95% of the PCa emerges from the glandular epithelial portion of the prostate, with progressive loss of the basal cells and in case of malignant invasion; there will be a rapture of the basement membrane. PCa incidence has a variable probability in different zones of the prostate, in 70% of the case the PZ is the origin of the adenocarcinoma, while the CZ and TZ have 25% and 5% probability of being infiltrated with the malignancy. Once the elation of the basement membrane occurs, there will be a higher possibility of metastasis to the surrounding organs such as SV, UB, penial and rectal tissues in less possible incidences [20]. Pathological fracture and sclerotic lesions of the bone particular the spinal bones is a typical sign of PCa metastasis that can be diagnosed by imaging, metastasis to abdominal and thoracic visceral organs can also occur in very rare conditions [21, 22].

Tumors originating from the muscular section of the prostate are very seldom and they usually occur with people with hematologic malignancies such as leukemia. Leiomyosarcoma and solitary fibrous tumors are examples [19].

The SCs of the prostate is the primary cellular sites for the manifestation of PCa, malignant glandular neoplasia. The pathogenesis of the carcinoma can be addressed starting from the stem cell, which differentiates all the way from a variety of intermediate precursor stem cells to the final SCs according to the hierarchical or stem cell model of PCa prognosis. The cells of the prostate are organized in a basal and laminal layer, while those cells of the basal layer contain a cell surface receptor which response to the growth factors (GF) produced by the smooth muscle cells of the FM section, only a small amount of this cells possess androgen receptor. Those that contain androgen receptor are considered the stem cells for the development of intermediate amplifying cells and later to SCs. When the stem cells are mutated or lost the succeeding intermediate SCs will be changed into malignant cells, and each cell type may differentiate in its own path to be the source of final PCa that leads to the heterogeneous characteristics of the malignancy [23]. Figure 2.3.1 shows normal cellular stratification and malignancy prognosis pathways.

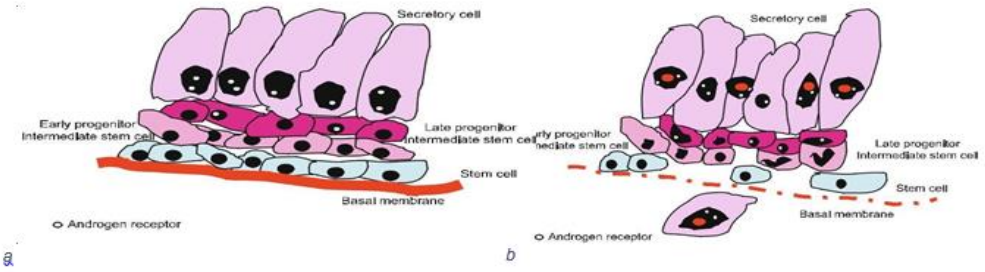

Figure 2.3.1 *a) Normal cellular anatomy of the prostate epithelium. B) The hierarchical model of tumorigenesis in the prostate gland. Steam cells will differentiate to progenitor cells and later de-differentiate to intermediate cells and finally to SCs. Mutation can occur at any stage of cellular differentiation and each cell type involved will take its own course of malignant transformation giving rise to the variable appearance of PCa [23].*

The cause of the transformation from the normal glandular structure to malignant foci is not clearly identified. Epigenetic, genetic and oxidative damage due to the response of the inflammatory cells secondary to infection is mentioned as a possible underlying factor for the prognosis of PCa. There is strong evidence that prostate atrophy secondary to inflammation caused by infection is a major factor for the development of PCa. Most of the prostate atrophic anomalies are associated with inflammation and most inflammations will cause intraepithelial atrophy [23, 24].

Inflammatory response due to infection will let the inflammatory cells to produce oxygen and nitrogen-based ions radicals when they combine with environmental factors such as diet they will cause oxidative damage that involves active oxygen and nitrogen species (ROS, RNS) being attached with the genetic material to lead to malignancy on the long run. Cells have a checkpoint mechanism to avert the effect of oxidative damage. The catalytic mechanism is used by cells to remove this active ion radical, develop a pathway to heal the damaged genetic material or in case of advanced DNA damage the cells will be forced to undergo controlled suicide. If the cells fail to defend themselves from this inflammatory damage, using the methods mentioned carcinogenesis would be initiated. Oxidative damage secondary to infection has a strong resemblance with the way cancer cells cause damage to the surrounding cellular structures. During oxidative damage to the cells, there will be higher expression of immune cells near the infection site, anti- apoptotic genome (BCl2), a higher expression of KI67 protein, an input for cellular prolifera-

tion, less expression of cell cycle checkpoints such as p27, increased presence of glutathione-S-transferase p1 (GSTP1) and cyclooxygenase-2 (COX-2). Oxidative damage will cause the atrophic change to the SCs and the process is called proliferative inflammatory atrophy (PIA) that occurs after successive infections, sudden cellular damage, immune complications and lack of oxygen due to vascular anomalies. Expression of GSTP1, GSTA1, and COX-2 are the manifestation of PIA. Despite the fact that there is 42.5% similarity between the contours of PIA and prostate intraepithelial Neoplasm (PIN) there are some non-uniformity to decide whether PIA is the antecedent for the development of PIN. That might be due to a low degree of correlation between the two lesions or poor structural similarity of the two [23, 25].Figure 3.2.2 microscopic appearance of PIA.

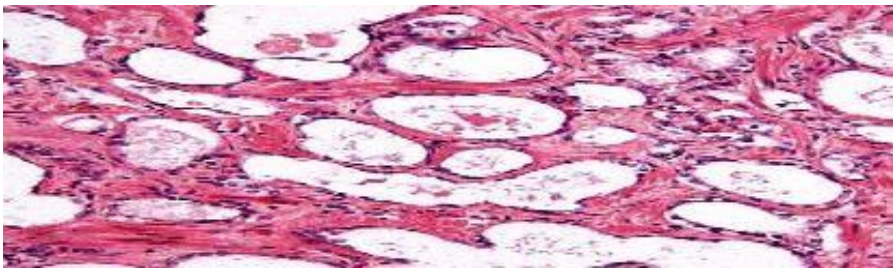

Figure 2.3.2 *Histologic appearance of PIA [23].*

PIN is a lesion associated with the uncharacteristic nuclear configuration and increased proliferation of the SCs with maintained basal membrane. Depending on the level of nuclear abnormality, PIN is classified into two types, the low-grade PIN (LGPIN) with a variant appearance from person to person and low specificity for the detection of cancer, due to this fact pathologists do not usually report on this type of PIN. The high-grade PIN (HGPIN) has a strong sensitivity to cancer detection (22-25%) on biopsy study while the low-grade PIN is within the18-20% range. HGPIN is not apparent on imaging or physical examinations, only histologic monitoring is the possible method for its diagnosis [23, 26]. Figure 2.3.3 shows the microscopic appearance of HGPIN.

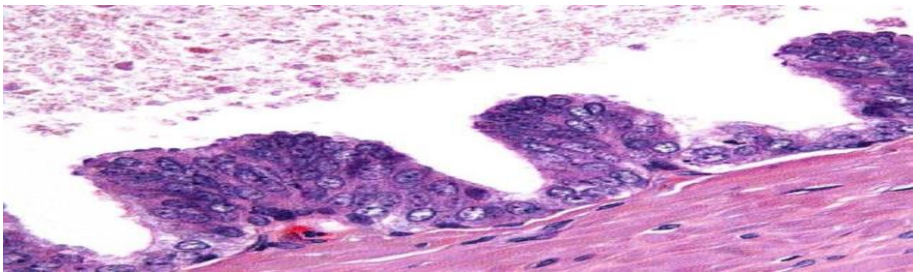

Figure 2.3.3 *Histologic appearance of HGPIN. The basement membrane is shown intact while the tall columnar SCs are transformed into malignant cells with the irregularity of the nucleus [23].*

The fact which makes the HGPIN as a predecessor to PCa is, in both cases, there is an increase in proliferation rate with time. in 70% of specimens studied during biopsy it was found to have similar contour, a disappearance of the basal cells and increased rate of nuclear abnormality and both have a similar expression of genetic molecules such as α-methylacyl-CoAracemase-AMACR)[23].Figure 2.2.4 shows steps of PCa prognosis

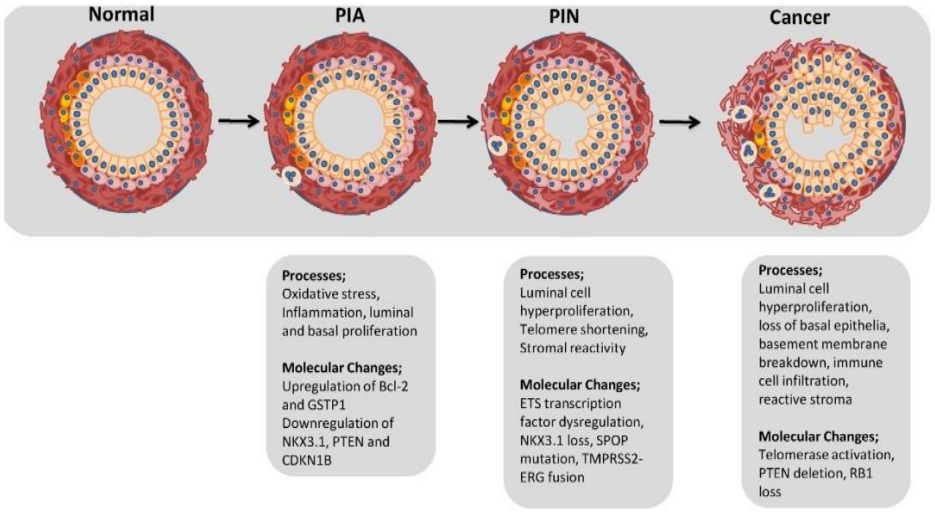

Figure 2.3.4 *Steps involved in the malignant transformation of normal prostate cells with the intermediate steps (PIA and PIN) and the processes happening [26].*

The other important factor for the development and carcinogenesis of PCa is androgen. Androgen belongs to a group of steroid hormone secreted mainly by testis and adrenal gland, and to a small amount by the peripheral organs including squamous cells and prostate gland. In a normal male, the function of this hormone is the development and specialization of reproductive organs and in a later age, it will initiate the onset and development of secondary sex behaviors [27].

Outside the intraProstatic environment, androgen is mainly contained as a form of testosterone. Out of the total volume of circulatory testosterone 44% of it makes a high affinity based binding with the sex hormone binding globulin(SHBG), 54% of it is making a low affinity based binding with a serum protein albumin. The remaining testosterone (1-2%) circulate as unbinding and free. Free testosterone from the circulatory system will diffuse passively to the cytoplasm of prostate cells, while the low affinity bound testosterone to albumin will make dissociation from it to pass to the intracellular environment the same way as the free testosterone. Once inside the cytoplasm testosterone make a one direction metabolism with the mediation of the enzyme 5α reductase to form dehydrotestestrone(DHT) . DHT will be attached by the intracellular receptor called androgen

receptor (AR) that will carry it to the cellular DNA inside the nucleus to attach it with an androgen-sensitive element to initiate the transcription of the genome that will trigger the proliferation and development of prostatic cells. The further action of DHT ceased by the catalytic action of enzymes 3α hydroxyl steroid and 3β hydroxysteroid to convert it to 3α androstanediol (3α-diol) and 3β androstanediol (3β androstanediol glucuronide) to be eliminated from the cellular environment[27].Figure 2.3.5 shows the physiologic pathway of androgen.

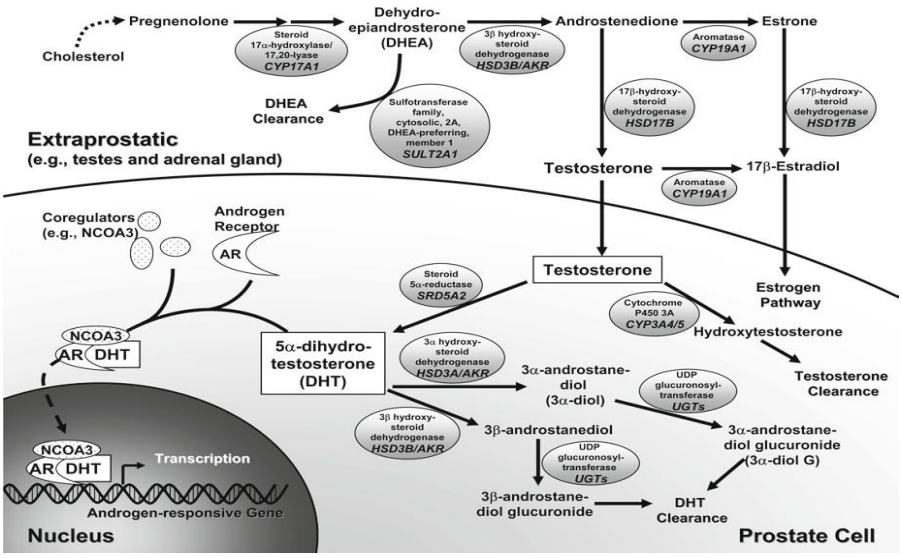

Figure 2.3.5 *Steps involved in the formation of testosterone inside the testis and adrenal gland and metabolic pathway of androgen (DHT) inside the prostate cellular environment leading to the action of androgen on prostate cells and its pathway of elimination form intraprostatic cellular environment [27].*

When the level of androgen is in a lower amount for instance during androgen replacement therapy, non-steroidal hormones such as estradiol, vitamin D and insulin-like growth factors (IGFs) can act as a ligand to activate the androgenetic effect on the prostate. The coactivator proteins such as ARA54, ARA55, ARA70, ARA160, p160, BRCA1, AIB1, and CBP boost the action of androgen by increasing the transcriptional efficiency of AR [27]. Although there is no direct relation between the level of circulating testosterone and the risk of developing PCa, most types of PCa are dependent on the presence of androgen for its development and prognosis, androgen deprivation therapy is the most effective method for the treatment of advanced tumors with higher initial treatment response. But later has a higher recurrence rate and aggressiveness, this is mainly due to a raised level of PSA, AR mutation and nonspecific ligands which increase the sensitivity of AR[27, 28].

In the early stage, the person may not experience any signs or symptoms of PCa, but as the disease prognosis is advancing, the patient will be presented with incontinence, the urinating blood (hematuria), difficulty or pain while urinating [29].

One or more of these signs and symptoms can be seen due to pathological conditions of the prostate such as BPH or other conditions arising from the surrounding organs and systems. In addition, in case of advanced conditions, the patient may experience back pain due to metastasis to the vertebra and can have associated pathological fracture due to osteoporosis.

2.4 Principle of ultrasound imaging

US is one method of imaging the internal body structures using non-ionizing high- frequency sound waves. The US enables the imaging of static and dynamic structures in real time setting [30].

Sound is mechanical energy that needs a medium to propagate from one point to another. When the sound wave enacts the particles in the medium, the particles will vibrate in their resting position and colliding with the adjacent particles transferring energy, the sequential compression and relaxation of particles is responsible for transferring sound energy from source to the destination. Depending on the relative direction of energy propagation and direction of particulate vibration sound wave is classified as a transverse or longitudinal wave. Only Solid mediums support transverse wave propagation [30].

Wavelength (λ), frequency (f), amplitude (A), speed(c) and period (T) are major parameters used to describe a wave.

C is dependent on the type of material medium being high in dense bodies than in lose medium , in general US propagates with an average speed of 1540m/s in soft tissues[31].

Naturally, occurring crystals (quartz, Rochelle salts, and tourmaline) and artificial crystals (zirconate titanate (PZT)) are used to produce and receive US. These materials have a capability of converting mechanical energy (sound energy) into electrical energy (piezoelectric effect) and vice versa (reverse piezoelectric effect) [32]. The crystals are contained inside a US probe (transducer), when an electric pulse is applied on the crystals they will create a sound pulse that will be directed into the body, then the transducer waits for the returning echoes before sending the next pulse. Each pulse has a duration of 1μs and created within an interval of 1ms. The crystals spend most of their time (99.9%) listening to the echoes than creating the sound waves that is 0.1% of the time. a single crystal that is rotated about a fixed axis at a rate of 1000-10,000rpm or a phased array of multiple crystals arranged and stimulated in a sequential fashion is used in US probe

to create a 2D screen image [30, 33].

As the US penetrates through the tissue, some of the energy is attenuated (absorption and scattering). Attenuation is dependent on the material property the sound is traversing and the frequency of the sound wave. In soft tissues, attenuation is directly proportion to the frequency and in liquids; attenuation is directly proportional to the square of the frequency [34].

As the sound wave reaches a boundary between two different structures, some of the energy is reflected and part of it will be transmitted. If the angle of incidence is greater than 60o, the reflected echo will be received by the transducer to create the image. The more intensity of reflected sound the brighter the image displayed [30].

Acoustic impedance (z) is a measure of the resistance of the medium particle to sound propagation. It is a product of the density (ρ) of the medium and velocity (c) of propagation through it. The amplitude of energy reflected at the interface is dependent on the difference of z between the tissues. The higher the difference the higher the amount of reflected energy and the brighter the image [35].Figure 2.4.1 shows principle of ultrasound operation.

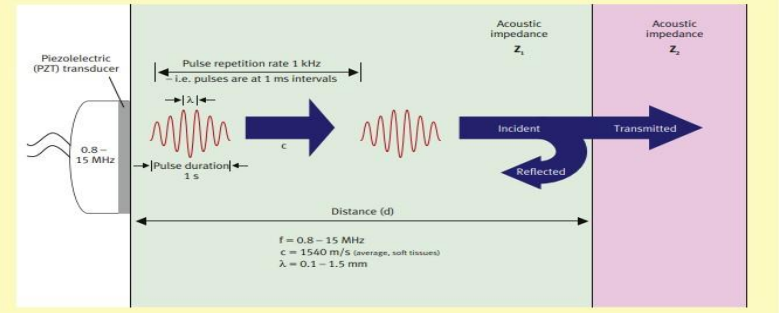

Figure 2.4.1 *Creation, propagation, transmission and reflection of US at different boundaries [31].*

Amplitude or A-mode is the display of the amplitude of the reflected signal with respect to time. The interval on the time axis is directly proportional with the depth of the surface the signal is emanated. The time it takes for a signal to reach the transducer is given by t=2d/c therefore the depth is given d= ct/2[30, 31]. Figure 2.4.2 show A-mode display.

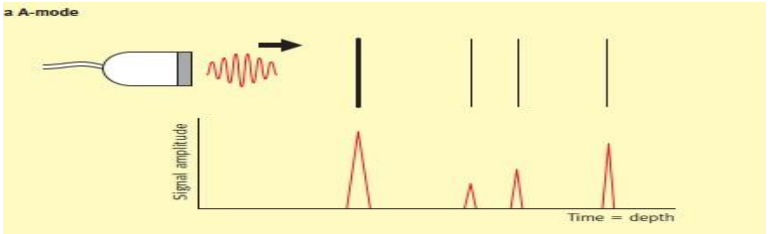

Figure 2.4.2 *The plot of signal against depth in A- mode operation [31]*

B-mode is another alternative of displaying the amplitude of the reflected signal as a brightness with respect to time (depth). The degree of the brightness is proportional with the amplitude of the reflected signal. B-mode image is created by moving around the sound pulse at 90^{o} with respect to the direction of the US beam. When this happens at frame rate of 20-40 per second, a visual dynamic image can be created [31, 34]. Figure 2.4.3 shows B-mode operation of US

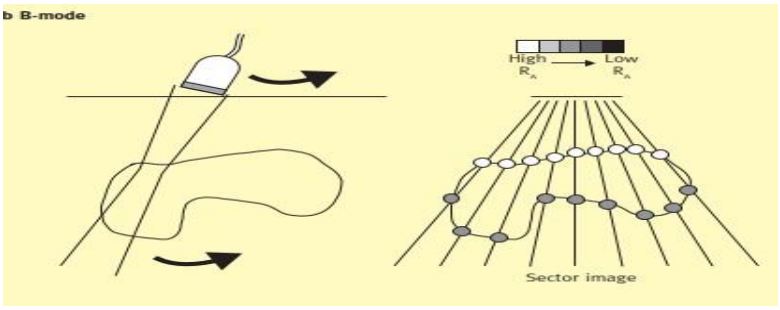

Figure 2.4.3 *B-mode operation of US in stationary underlying structure. RA is the ratio of reflected sound pressure and incident sound pressure [31, 35].*

By mounting a transducer at a fixed position on top of a dynamic underlying structure, it is possible to see the movement of structures with respect to time and this is called motion (M-mode) mode [31]. Figure 2.4.4 show principle of M-mode operation.

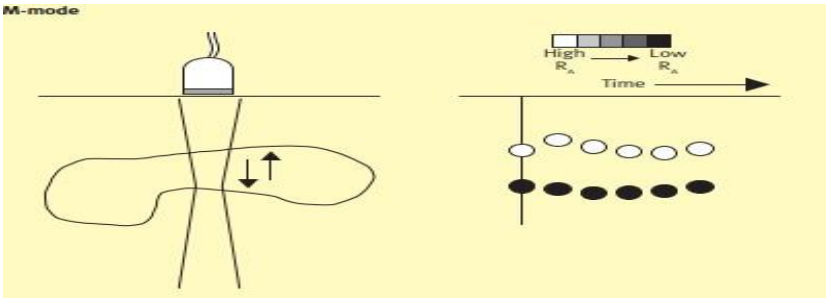

Figure 2.4.4 *Principle of M-mode operation during a mobile underlying structure [31].*

2.5 Texture analysis

Image texture is described by the display, form, and arrangement of part of the image. Image texture analysis method by using MaZda will lead to obtaining useful information about the underlying physical object (biological structures) [36, 37] A digital image is a composition of small rectangular blocks(picture elements or pixels) in case of 2D and

voxels(volume elements) in case of 3D pictures which are represented by a gray level value. The allowed grayscale values a pixel can have is within the range of 0 to 2b-1, where b is the number of bits of the image. Texture analysis is attributed to an assessment of the pixel gray level values and their interrelationship in the image [37].

Multiple steps are involved in MaZda image texture analysis. Image acquisition (2D or 3D) is the first step. Windows bitmaps and DICOM are the supported formats to be loaded in Mazda [36].MaZda has an option to analyze the whole image at once or to choose a specific region of interest (ROI). The results will be displayed as feature maps or a text list of features vectors and each way has its own purpose [36]. Figure 2.5.1 shows the process of image analysis steps in MaZda.

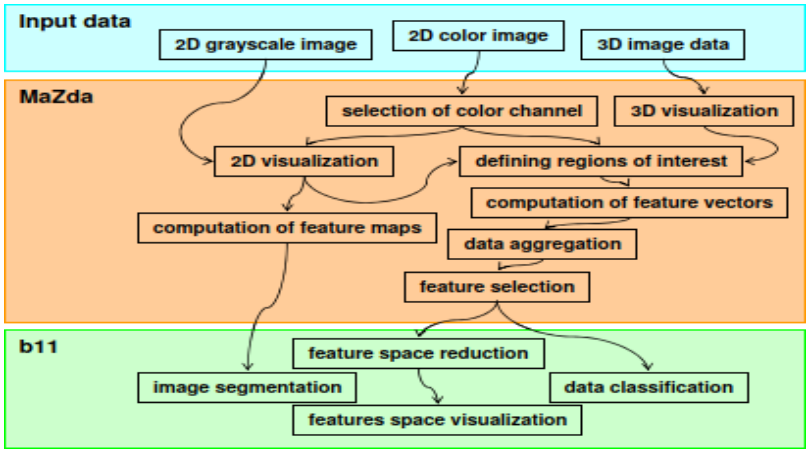

Figure 2.5.1 *Steps involved in image texture analysis using Mazda [38].*

Statistical, model-based, structural and image transform methods can be used to analyze the pixel gray level values and their correlation. Each method has an advantage and disadvantage over the other but on this thesis, we have used a statistical method of analysis.

The statistical method describes the texture features based on the distribution and the interrelationship of the pixel gray level values [37]. The main texture parameters evaluated in the statistical method of texture analysis are histogram that is calculated from the gray level of the pixels excluding the interrelationship with the rest of the pixels in the image. The main features are mean, variance, skewness, kurtosis, and percentiles [37]. Simply histogram counts the number of pixels that have the same gray level value and display it in the x-y plane where the x-axis shows the gray level value and the Y-axis shows the number of pixels with the same gray level values. Figure 2.5.2 histogram display of pixel gray level values.

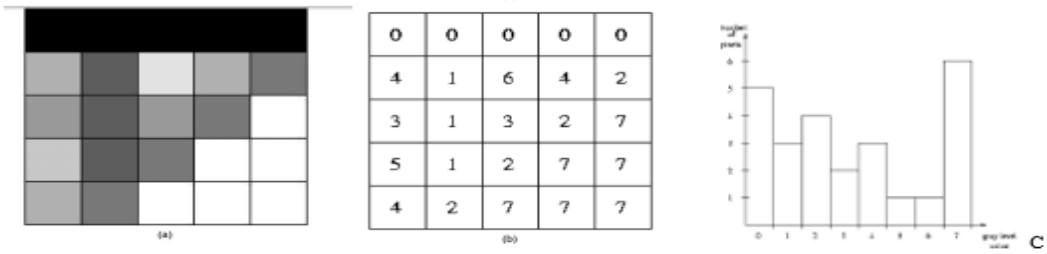

Figure 2.5.2 *a) An image with the 5x5 pixels having a gray level value between 0 to 7,b) depiction of the gray level values of the pixels. C) The corresponding histogram representation [37].*

Co-occurrence matrix (COM) is derived from the gray level values of a pair of pixels that means it is a second derivative histogram. Contrast and entropy are the parameters calculated from COM, while contrast describes the gradient of the pixel gray level values, entropy asses how the pixel values change within a given distance of the image. The value of entropy is higher if there is an abrupt change of gray level values within a given distance means that it is a measure of randomness or disorder in the image [36, 37].

Run length matrix (RLM) is a count of pixels with a given gray level values and length. Horizontal, 45^{o}, vertical and 135^{o} are the run-length matrices that are used by MaZda. A fraction of the image (amount of pixels that are included in a given run) and short-run emphasis (a portion of runs that have short run length) are the main parameters executed by RLM [36, 37].

Absolute gradient asses the rate of change of pixel gray level values within the image. If the gray level values are changing promptly, we have a higher absolute gradient. The values may be assigned either positive or negative depending on the route of transition from black to white or white to black. Mean and variance are the parameters derived from the absolute gradient. Figure 2.5.3 MRI image display of the absolute gradient matrix.

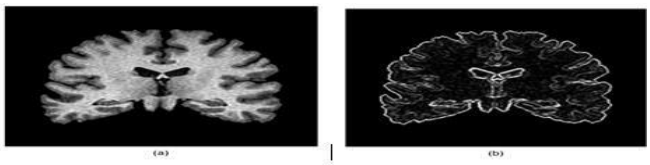

Figure 2.5.3 *a)T1 weighted coronal section of the brain. b) Absolute gradient image it shows the sharpest contrast on the areas where the gray level value difference are higher [37].*

3. DIAGNOSTIC METHOD FOR PROSTATE DISEASE

3.1 PSA tasting

PSA testing has given a new dimension for detection, management, and monitoring of PCa. The disease prevalence is increasing since the implementation of PSA screening in 1986. The use of PSA testing has enabled the early diagnosis when the disease is only localized to the organ that will have a high treatment response and increased probability of mending the prognosis. The rate of diagnosis at a later advanced stage with regional invasion has declined by 75% since 2003 [21, 39].

PSA has approval for PCa detection since1994 by the United States food and drug administration (FDA). Even though PSA testing has made a dramatic improvement in the overall detection of PCa and decreased mortality rate due to the disease, there are still discrepancies among clinicians who question the justification of the method. This is partly because PSA enables the detection of early tumors that does not cause any functional deformity to the person, and does not certainly need treatment and the associated complication in the urinary, sexual and gastrointestinal (GI) especially rectal mobility after any kind of therapeutic procedure followed [39].

Both normal prostate tissues and cancerous tissues secrete PSA and release to the seminal fluid to change the semisolid form of semen to motile liquid form and some part goes to the circulatory system. In normal condition, only a small amount of PSA is present in the circulatory system this is due to the anatomic architecture of the prostate to maintain most part of PSA to remain inside the glandular section. Out of the circulatory PSA, only around 20% on average is present as free without any binding with other constituents, while around 80% of it is present as binding with protease inhibitors (α1- antichymotrypsin) and stay as indolent. The PSA level measured is the sum of both bound and free serum amounts [39, 40].

The variation in the proportion of circulatory PSA spring from the change in the structure of the gland secondary to diseases prognosis (PC, BPH or prostatitis) or due to some (invasive) procedures such as TRUS guided biopsy, catheterization, DRE and surgery near the vicinity of the gland. External factors such as genetic background, age, and physical fitness also contribute to the change in the level of PSA. [21, 39]. The non – cancerous conditions are the major factors to increase the rate of false-positive results during PSA measurement. If a person is on androgen inhibition therapy using finasteride the level of serum PSA will dramatically be decreased and the red out should be doubled

for considering further steps in order to decrease overdiagnosis and overtreatment [40].

The level of circulatory PSA indicates the risk of associated malignancy. In the previous read, up to 97% of normal males who are at their 4th decade or above had a PSA level of less or equal to 4ng/ml, based on this the lowest level of PSA to undergo biopsy was set at 4ng/ml. This value has false positive diagnostic results in 63% of cases and false negative results in 9% of cases. PSA level in the range of 4-10ng/ml has a 75 % false positive result for the presence of malignancy [39].

Although peoples who have a PSA level less than 4ng/ml does not undergo a biopsy to confirm the presence of PCa, it is reported that there is a 15% incidence of high-risk malignancy in those who have a PSA level between 0.5 -4ng/ml. One way of accommodating these errors might be to lower the threshold value to increase the detection efficiency but in contrary, it will also incline to false positive results and decrease patient comfort and waste of resource due to unwanted biopsy and overdiagnosis/overtreatment [39].

PSA level also varies with age and on average it will increase linearly with age especially after the 5th decade. Common values of PSA in different age groups of normal peoples has been established. The measured value of PSA from a given person is compared with this age-specific normal values in order to increase sensitivity in young male and specificity in older men. By doing this overdiagnosis/overtreatment can be decreased and unnecessary biopsy can be avoided [39, 40].table 1 shows normal PSA values in different age groups.

***Table** 1 Age-specific PSA threshold values [39].*

age	Normal(ng/ml)
40-49	0-2.5
50-59	2.5-3.5
60-69	3.5-4.5
70-79	4.5-6.5

This value has shown to miss 40% of the malignancies on average and they are not widely accepted as a prior means of diagnosis. In general, PSA testing is not accurate and differential diagnosis from the other pathologies conditions, which also increase the level of serum PSA, cannot be solely confirmed. PSA can be used to follow up a newly diagnosed PCa to assess the grade and risk of the malignancy and after treatment follow up to assess the treatment response and the probability of relapse and the need for additional management to be used[21, 39].

In order to make a differential diagnosis between BPH and PCa using PSA, a new method called PSA density (PSAD) is used. PSAD accounts the volume of PZ where most of the

PCa is common and volume of TZ that is common for BPH manifestation. The measured circulatory PSA value is divided over the volume of TZ or PZ measured using TRUS. For PCa the minimum values that lead to biopsy analysis are set to be in the range of 0.1-0.18ng/ml/cm3. BPH is predicted when the PSAD is between 0.23-0.38ng/ml/cm3. PSDA can also predict the grade of the tumor and can be used as a follow-up procedure to predict the treatment effectiveness. PSA to volume ration enables both prediction of PCa and differentiation from BPH. Higher PSA/volume has a strong association with PCa and if the gland is above 40gram and the PSA is in the range of 4-10ng/ml there is 80% accuracy for BPH diagnosis than PCa [22, 39].

The reason PSAD is not popular is that it is invasive procedure decreasing the patient comfort; accurate measuring of the prostate volume may depend on the personnel skill and experience and depend on the architecture of the gland. In addition, the economic aspect of the procedure is not good [41].

The susceptibility of being diagnosed with PCa in the future can be estimated by PSA velocity (PSAV). PSAV measures the rate of change of PSA level per time. In those, whose PSA level is measured between 4-10ng/ml and if they have PSAV of 0.75ng/ml/year, there is 79% probability to develop PCa and 90% accurate differential from BPH. PSAV is directly proportional with the serum PSA level, PSAV values between 0.1-0.5ng/ml/year are set to be the value to initiate biopsy study [39]. In order to avoid the variation of PSA due to normal physiologic activities and nonmalignant pathologies during the measurement period, there should be enough time intervals of measurement before the biopsy is followed. PSAV is used as a post-treatment assessment method to address the treatment response, probability of relapses and aggressiveness of the malignancy [41].table 2 shows PSA values and PCa risk.

Table 2 *Probability of exposure to cancer based on PSA and percentage of free PSA [39].*

PSA (ng/mL)	**Probability of Cancer** (%)	**% free PSA**	**Probability of Cancer** (%)
1.0 - 3.0		< 20	11
4.0 – 10	25	0-10	56
		10-15	28
		15-20	20
		20-25	16

3.2 Ultrasound imaging

US is the ideal first-hand diagnostic modality in genitourinary radiology. US is the prime choice of radiologists to access the genitourinary pathologies in real time and during an interventional procedure for treatment (aspiration), US-guided surgery and extraction of biopsy without causing unwanted complications due to normal parenchymal damage and associated hemorrhage due to misplaced aspiration or biopsy needle[42]

Elevated PSA values and abnormal DRE results are the main indications for performing TRUS and TRUS guided biopsy for PCa diagnosis. The contraindications for the TRUS guided biopsy are mainly sever rectal hemorrhage, abnormal immune reactions, acute prostatitis and rectal ablation [43].

Grayscale TRUS is the main diagnostic tool for the initial evaluation of prostate with the elevated PSA and abnormal DRE or during the presence of sign and symptoms related to the UB abnormality. TRUS can depict the anatomic detail of the gland and the surrounding structures well using a high frequency (5-7.5MHz) transducer. We can obtain a high-resolution image for evaluating the gland for the presence and local staging of PCa, BPH, and infections [44].

Accurate volume measurements can be done using TRUS for calculating PSAD that will give a clue between PCa and BPH. Transverse (height) and anteroposterior (width) of the prostate is measured using axial scans and since bladder obscures the base of the prostate, we cannot see the full length of the gland on axial scans and have to use sagittal scans to measure longitudinal dimensions (length). A prolate ellipsoid formula is mainly used to calculate volume [11].Figure 3.2.1 normal prostate ultrasound images.

$$Volume = height \times width \times length \times 0.52 \text{(a prolate ellipsoid formula)}$$

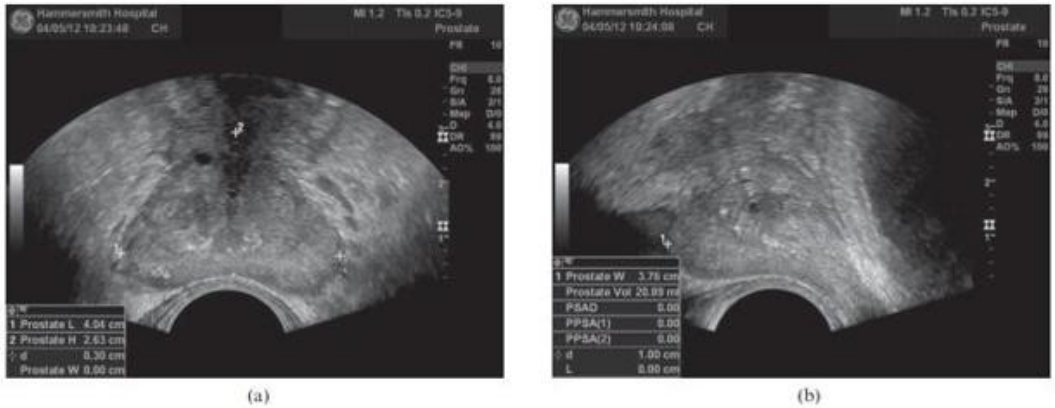

Figure 3.2.1 *Axial (a) and sagittal (b) TRUS scan of normal prostate for measuring volume [3].*

Evaluating prostate for PCa using TRUS is mainly assessing if there is any structural abnormalities, low echogenic foci, and abnormality of the fibrous capsule (bulging or irregularity).the structural findings are not very conclusive information for accurate diagnosis of PCa. TRUS guided biopsy has to be taken from the area of the prostate that is mainly susceptible to the malignancy and any suspected area during TRUS for further analysis [3]

TRUS is an important means of directing prostate intervention (biopsy). The indication for this procedure is the same as grayscale TRUS. The patient being in decubitus position the US probe is inserted inside the rectum to guide an 18G biopsy needle in the region of interest. Samples are taken from six sites of the PZ in a symmetric manner (right and left apex, right and left mid gland and right and left base). Samples can also be taken from any part of the gland if there is suspected PCa echo signal in order to increase the sensitivity and limit repeat biopsy request [11].

Although TRUS guided biopsy remains to be the routine procedure to detect PCa it has its own limitation. Since samples are taken from a specific area of the gland, there is a higher probability of missing the malignancy and there is always a possibility of repeat biopsy this is in addition to the sampling mistakes that might be dependent on the experience of the operator. In the first trial, there is a 60% probability of false negative results. However, as the number of repeat biopsy is increased the rate of false negative results might decrease. This is the main reason that the traditional six core sampling is becoming insufficient to make an accurate diagnosis and has to be increased to 10 or 12 cores [11].

Since aseptic methods are not used during TRUS, Infection prevention before and after biopsy are managed by using antibiotics. Prophylactic antibiotics are generally administered before the procedure. Fluoroquinolones with higher tendency to diffuse inside the prostate tissue are used to prevent infections after the procedure mainly because of Escherichia coli. A cleansing enema is also used before the procedure in order to remove the fecal material to reduce the probability of microbial invasion through the needle path [42, 43].

US-based interventions require choosing the best route for inserting the probe that makes the distance between the biopsy needle and the anomaly minimal and avoiding the intermediate structures interfering with the sonic window. The biopsy needle has to have a shorter travel distance in order to decrease the risk of unwanted structural damage and associated hemorrhage that might in Sevier case leads to the secession of the procedure and emergency management may follow. The path of the biopsy needle has to be within the range of view and the signal from it should not be superimposed with the signal from

the prostate tissue or pathologic echo signals [42].

Color or power Doppler US can also be used to demonstrate the vascular characteristics of the prostate. In non-pathologic conditions, the prostate has a limited Doppler signal but if it is infiltrated with malignancy there might be a prominent increase in the microvasculature. The strength of the Doppler signal is directly proportional to the aggressiveness (grade) of the tumor [11]. If the conventional TRUS has shown no sign of malignancy we can use color/ power Doppler to detect if there increased vascular density and asymmetry in the vascular distribution [3].Figure 3.2.2 gray scale and Doppler US of prostate.

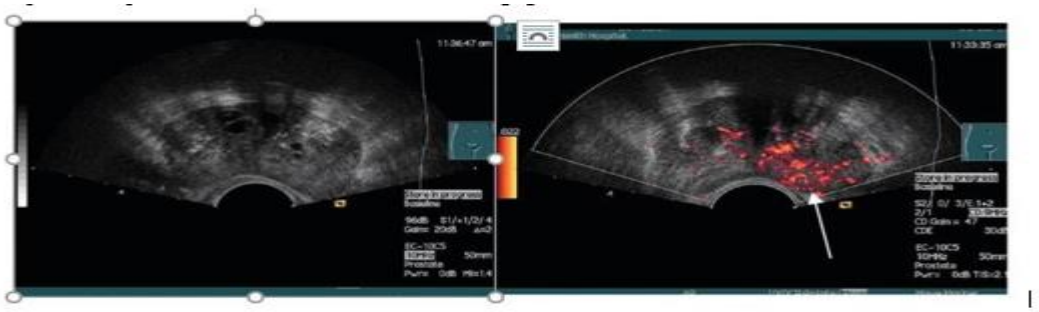

Figure 3.2.2 *a). Normal axial TRUS scan of prostate with no suspected area of malignancy). b) Doppler US of the same scan with increased vascular density and asymmetry (arrow). Biopsy has confirmed malignancy [3].*

Doppler/power Doppler increase the sensitivity of PCa detection by up to 10% but it still cannot totally replace biopsy since some cancers have shown no vascular signals and in the contrary nonmalignant anomalies can be present with increased vasculature [3].Figure 3.2.3 Doppler US of prostate

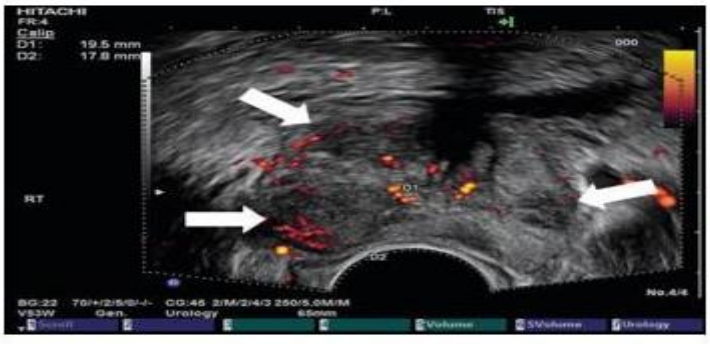

Figure 3.2.3 *A 68 year old patient with abnormal PSA value and with no clinical signs and symptoms. Axial scan showing multiple low echo signal foci (arrow) with increased vascular density resembling PCa. Biopsy has confirmed there is no malignancy [3].*

Elastography is one of the recent diagnostic tools to differentiate normal from the abnormal tissue parenchyma by using a physical means (compression) using US transducer as a means of applying deformation and measuring the stain (stiffness) of the tissues. Different pathologic conditions have a variable strain response and that will be used to make a differential diagnosis between cancerous and non-cancerous tissues [45].

It enables to discriminate separate tissue structures based on their variation in stiffness and this will be represented as color code together with a B-mode display of the same tissues. It measures the stiffness using elastogram and the results will be compared with the confirmed strain of malignant samples obtained by prostatectomy. The method has a very high efficiency of up to 74% to rule out malignancy with a smaller volume of less than 1ml and the accuracy can reach 100% in case of tumors with a volume of greater than 5ml [46].

Elastography has been also used to guide biopsy extraction showing an increased sensitivity than the conventional methods by 7.1%. It has also increased the advantage to detect PCa in patients with lower PSA values between 1.25 to 4 ngml-1[47].Figure 3.2.4 show elastogram of prostate and grayscale TRUS.

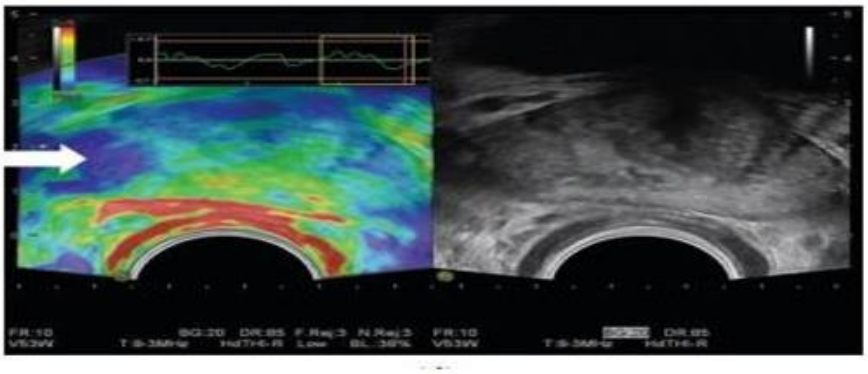

Figure 3.2.4 *Axial elastogram scan of prostate showing an increased stiffness on the right side of PZ (arrow). Biopsy has confirmed grade 7 carcinoma [47].*

Even though the method has an added advantage for diagnosing PCa it is not popular due to its drawbacks. The personnel should have a higher competence and experience to identify an area where to apply stress (in order to identify a strain response due to suspected carcinoma) since it is not possible to see the spot. This will cause a production of non-uniform scans making it harder to choose a biopsy site [45].

Contrast-enhanced color Doppler US is also used to demonstrate the smaller and larger blood vessels of prostate by administering a miniature contrast agents by intravenous (IV)

route. It has been observed that contrast enhanced US guided biopsy has a higher sensitivity than the conventional TRUS guided biopsy [48].Figure 3.2.5 show TRUS versus Contrast-enhanced color Doppler US of prostate.

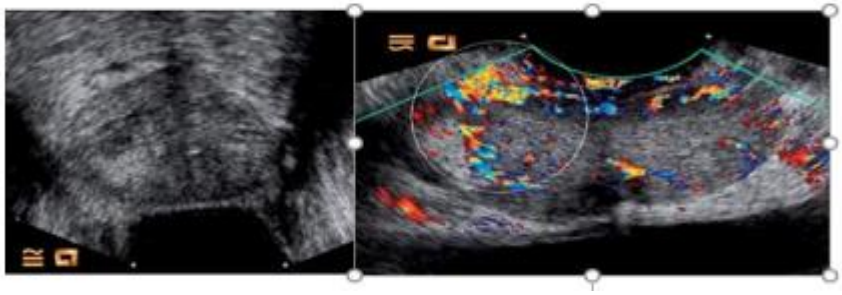

Figure 3.2.5 *a) A 57-year old axial TRUS with 4.8 ng/ml PSA with normal appearance of the prostate, contrast-enhanced US, b) Doppler US of the same person with asymmetric vascular distribution with prominent in the right side of Prostate [46].*

A more accurate biopsy extraction and better staging of PCa is possible using magnetic resonance imaging (MRI), which has a superior capability to show anatomical details. The biopsy needle can be placed in a more accurate position by using MRI guidance than TRUS alone. It also enables to document the sampling site that can be used as patient history in case of repeat biopsy or future treatment. MRI-TRUS fusion technique used the combined capability of both modalities to minimize the sampling error associated with TRUS-guided biopsy alone [49]. MRI guided biopsy is not without limitations. The use of a magnetic field makes the procedure complicated, it needs a method to reduce motion artifact and it is much more expensive [49]. Figure 3.2.6 shows the TRUS and MRI images of the prostate.

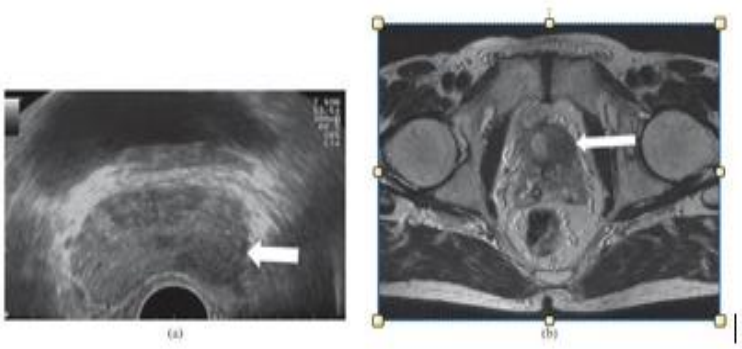

Figure 3.2.6*(a) Axial scan of prostate showing a nodular echo poor lesion on the left side of PZ with extension to the fibrous capsule (arrow), (b) T2 weighted axial MRI (b) confirms stage T3a with capsular extension with no involvement of left SV (arrow) [3].*

3.3 Normal ultrasound appearance of Prostate

TRUS can produce a good diagnostic detail of the prostate by placing the transducer at a possible minimal distance from the gland. In non-pathologic condition, the PZ will be seen as a smoothly echogenic or hypoechoic structure while the central part of the gland (CZ, PZ) can appear either uniformly isoechoic or hyperechogenic area and they may not be seen in clear-cut. The echo signal from PZ is variable between younger and older people being composite in older people and uniform in younger ones. TZ is enclosing the prostatic urethra and seen as echo poor region the same as the AFMS on the anterior aspect of the gland. The fibrous capsule makes a hypoechoic boundary between the prostate and the surrounding structures [11, 50].

Non-pathologic SVs are depicted without asymmetry with a faint-wall and echo poor internal signal. They can have a length in the range of 2.5 to 3.5cm with a thickness in a normal range of 1.1cm to 1.9cm. VD is seen as a tubular structure with a prominent wall than the SV and seen on the superior and more medial aspect than the SVs [50].

PZ constitute the largest of the gland volume and this will decrease proportionally with aging. The mass effect from the development of BPH in the TZ will make the TZ appear as a smaller size. By using the longitudinal section, we can visualize the ED as higher echo signal within the central part of the gland. NVB is seen on the posterolateral aspect of the gland in both sides with a triangular appearance in the middle of SV and prostate with a lower echo signal [47]. Figure 3.3.1normal axial and sagittal scan of prostate.

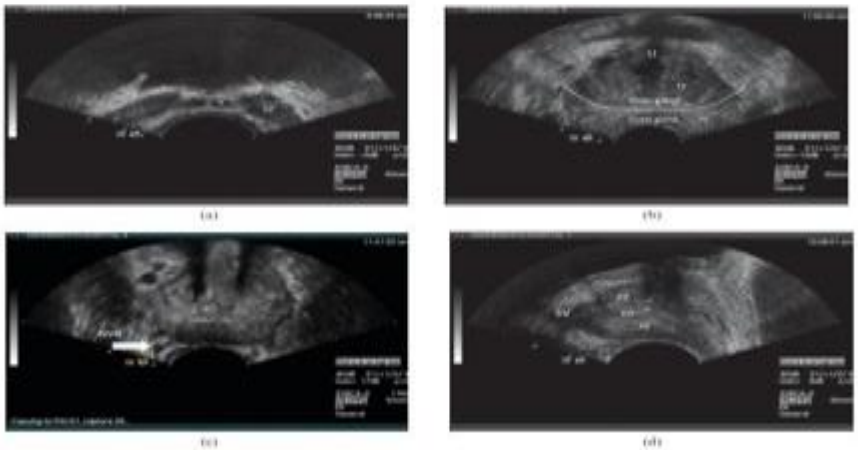

Figure 3.3.1 *Axial (a-c) and sagittal(d) TRUS of normal prostate*

with detailed normal anatomic structures, vas difference, NVB, neurovascular bundle, u, urethra , sv, seminal vesicles, cz central zone,pz, peripheral zone,ED, ejaculatory ducts[47]

3.4 Pathologic finding of Prostate ultrasound

3.4.1 Prostate cancer (PCa)

TRUS can rule out PCa accurately in up to 60% of cases with a correct differential diagnostic rate of 6%. There is a variable rate of PCa incidence in different zones of the prostate, in a majority of cases (70%), the malignancy is apparent on the PZ, in less extent (20% of cases) on the CZ and the reaming rate on the TZ. 60-70% of confirmed PCa has a low echo signal, with a confined and nodular structure in 30% of cases and in up to 50% of cases, it has an irregular and ill-defined pattern. Of the echo poor findings on TRUS, only 17-57% are malignancies [47]. In 40% of cases, PCa can have the same echo signal as the PZ and only 1% of the malignancies have echogenic appearance [11, 51].Figure 3.4.1.1 below shows PCa on TRUS.

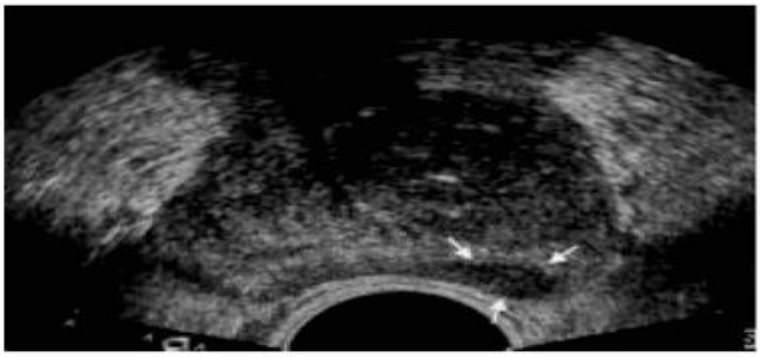

Figure 3.4.1.1 *TRUS scan of 65 year old with a well-defined echo poor carcinoma on the left side of PZ (arrow) [50].*

During metastatic conditions the prostate capsule will be seen as having an irregular edge, the ventral aspect of the fat section will be seen as having obliterated contour. SV can be seen if they are infiltrated with the carcinoma. TRUS can rule our extracapsular infiltration specifically in 50-92% of cases and for SV infiltration, it can have a sensitivity in the range of 22-60% with 88% accuracy [11].

3.4.2 Benign prostatic hyperplasia(BPH)

BPH is a pathologic condition arising from solely the glandular section of the prostate. It mainly involves the TZ and only 5 % of cases involve the periurethral zone. BPH can cause most of the time the hypertrophy of the prostate but it can also be apparent without

enlargement of the gland. On the US the TZ will be seen enlarged and will be clearly discriminated from the rest of the zones [50].

Sonographic findings may vary from well-defined nodular structure to diffuse hypertrophy of the central gland depending on the pathophysiology involved. Frequently CZ and TZ will have a less echo signal than the PZ but the central gland can also have a non-uniform echo signal. If BPH causes a mass effect on the rest of the gland we can observe the CZ and PZ with reduced size and demarcated from the TZ with an echo poor fat capsule, calcifications secondary to the BPH are observed on the wall of the fat capsule [11, 52].

Rarely BPH can be presented as a multifocal nodule with a variable sonographic signal but most of them will have poor echo signal. The US cannot differentiate these nodules from PCa but their areal involvement can give an initial prediction of their source [50]. Figure shows the most typical sonographic presentation of BPH.

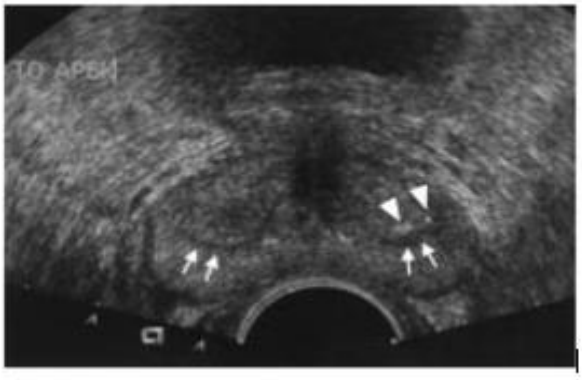

Figure 3.4.2.1 *Axial scan of 65 year old with BPH. Central part of the gland is separated from the rest of the gland by a hypoechoic fat capsule (arrow), hyperechoic calcification following the wall of the fat capsule are seen (arrow head) [50].*

3.4.3 Prostatitis

Prostatitis is mostly seen in younger males with acute or chronic inflammation of prostate secondary to pathogenic infections [47]. On US acute prostatitis will cause the enlargement of the prostate with uniform low echo signal because of edema formation. If color Doppler there will be increased vascular perfusion but these findings are not totally conclusive of the inflammation and the findings have to be compared with the patient clinical presentation. In advanced case there will be a well-defined mass with low to non- echo

signal, this is due to the formation of abscess [50].Figure shows grayscale TRUS and Doppler US of prostate.

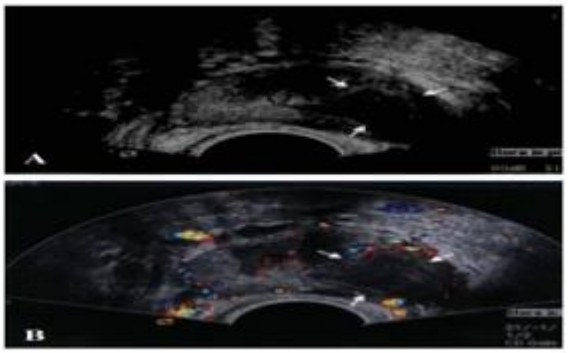

Figure 3.4.3.1 *(a) Axial scan of gray scale US shows a low echo signal mass on the right side of prostate, (b) Doppler US of the same person with increased vascular density around the mass [50].*

In the case of chronic inflammations, the US findings have a different appearance than on acute prostatitis. The echogenicity of the gland will be diffused, hypoechoic rim line on the PZ that is most common finding of chronic inflammation, low echoic nodular structures with a well-defined or diffused wall similar with the appearance of PCa and appearance of the hairline low echoic rim on the outer edges of the gland [50]. Figure shows US appearance of prostatitis on gray scale US.

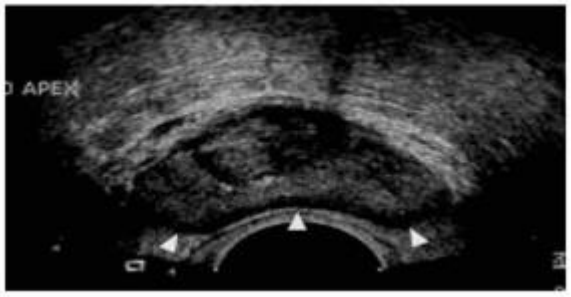

Figure 3.4.3.2 *Axial scan of 47-year-old prostate with a prominent manifestation of chronic prostatitis (arrow head) [50].*

4. MATERIAL AND METHODS

4.1 Images for the analysis

Multiple prostate US images (axial and sagittal) that were obtained in real clinical procedure were provided by Tampere university hospital in accordance with the hospital rules and regulation of confidentiality and purpose for academic use.

Axial scan of the prostate that shows normal structural detail, normal anatomic dimensions and without abnormal radiologic signal is chosen for the analysis in order to describe the normal texture features of the gland.

Random sample that shows multiple well defined hypoechoic nodular structures on the PZ were chosen initially and texture analysis was done separately and comparison of statistical parameters from different samples that have a similar echo appearance on the same zone of the gland (PZ) was done in order to discern if there is a correlation on the given parameters.

Samples that show low echogenic areas outside the PZ or in the CZ were analyzed and comparison was done with the parameters of the similar echo structures seen in the PZ. Sample scan that has multiple nodular hyperechoic foci was used for the analysis and the results were compared with the previous analysis.

4.2 Analysis procedure

The analysis procedure proceeded from analyzing the normal texture features (parameters) of Prostate mainly targeting the PZ where the incidence of malignancy is higher. The normal texture parameter results were used for comparison purpose with the texture parameters obtained from other similar scans from a different patient where the PZ has one or more abnormal echo signal. In each case, all four statistical parameters are analyzed before drawing the conclusion.

Two US scans with similar echo signal areas on the PZ were separately analyzed and the results were compared in order to draw any similarity between the texture features. The main objective of this method of analysis was to formulate standard reference texture features that might be used for comparison purpose for the future similar areas we might encounter from a different patient. For this thesis work, we mainly focus on comparing hypoechoic areas on the PZ of multiple scans since PCa is mainly apparent as a hypoechoic nodular area on the PZ.

Next, we have chosen US images which have shown a hypoechoic are on the central part of the gland. The results are compared with the similar echo signals that were shown on the PZ of the gland. This analysis was intended to draw if there is any similarity between the hypoechoic areas on the central part of the gland and PZ. Hyper echoic areas located on the gland have been analyzed. We have set a variable number of ROI selection and the results have beencompared with each other.

5. RESULTS

5.1 Analysing normal texture features of Prostate PZ.

For this procedure, we have chosen a sonogram (image 100349_0000.dcm) that shows a normal dimension and structural detail of the prostate and there is no sonographically visible abnormal signal detected. Figure 5.1.1 shows an axial scan of prostate sectioned at the mid gland with normal looking echo signal.

Figure 5.1.1 *Sonographically, the gland has normal dimension* (W=41.9mm, H=30.1mm) *and structural details. The PZ has a uniform echotexture (confirmed from texture analysis), the central part of the gland has a normal looking echotexture*.

By choosing a random region of interest (ROI) on the PZ we are going to execute the texture parameters and see if the results concede with the sonographic “normal appearance”. For this purpose, we have chosen three standard ROIs on the PZ. Each ROI is displayed with a different color and the color of the histogram is the same as the respective color of ROI. For this particular demonstration, we have set all ROI on the PZ but the same procedure can be applied on any section of prostate. Figure 5.1.2 shows chosen random ROI on the PZ of the prostate.

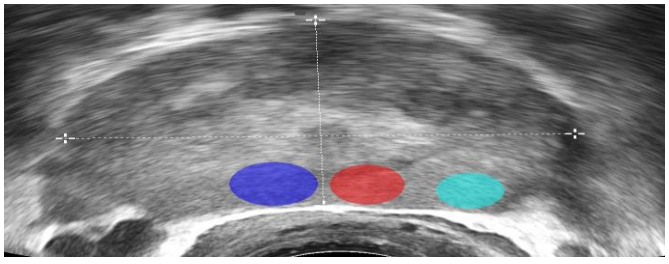

Figure 5.1.2 *ROI selection on the PZ of prostate. The first two ROI are set in more symmetric manner near the right and left mid PZ and one ROI is set on the left lateral aspect of the PZ.*

In practical situations, it is a good idea to place all the ROIs in a symmetric fashion in order to get the result interpretations more accurate. We expect the symmetric ROI to have a strong correlation in all types of texture parameters if the PZ is non-pathologic as assumed initially.

Before we proceed with the results of the texture parameters, theoretically if the PZ has no pathologic conditions we expect the ROIs to have a same or very similar results, and if we have set our ROI in a symmetric manner then we expect even more strong similarity between the symmetric ROI than the non-symmetric ROI.

Age and the clinical presentation should always be in mind before, during and after the analysis. Knowing the age is important on this particular analysis; PZ has a uniform echotexture in young people than in old people. If there is ROIs parameter difference and if we would have known, the person is relatively young then we can assume that the variation is due to abnormal conditions than in old peoples.

Histogram-based texture parameters have shown a strong correlation on the maximum and minimum luminosity of the ROI. Figure 5.1.3 shows Histogram of the ROIs with similar texture luminosity (maximum and minimum).

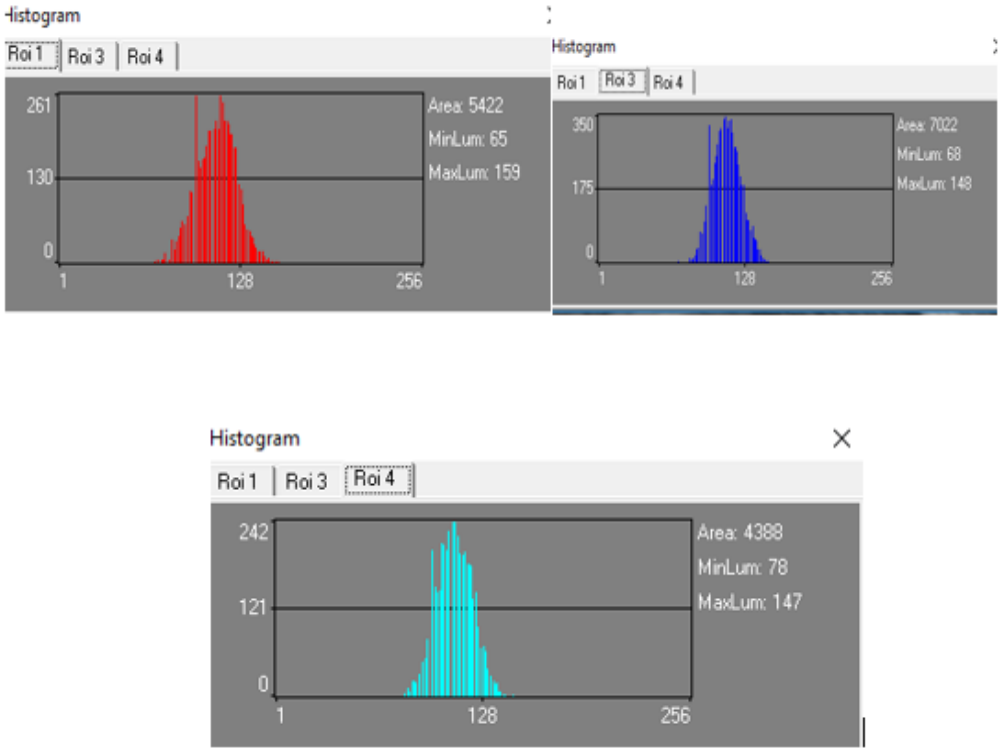

Figure 5.1.3 *Histogram based texture parameters without significant variation on the maximal gray level and minimum gray level values of the pixels in the respective ROIs.*

By roughly observing, the histogram charts we can see that there is no major variation on the histogram based texture parameters of the chosen three ROI. However, we can further analyze the mean, variance and percentile of the histogram based texture parameters to confirm our initial guess. Figure 5.1.4 shows the report window for histogram based texture parameters.

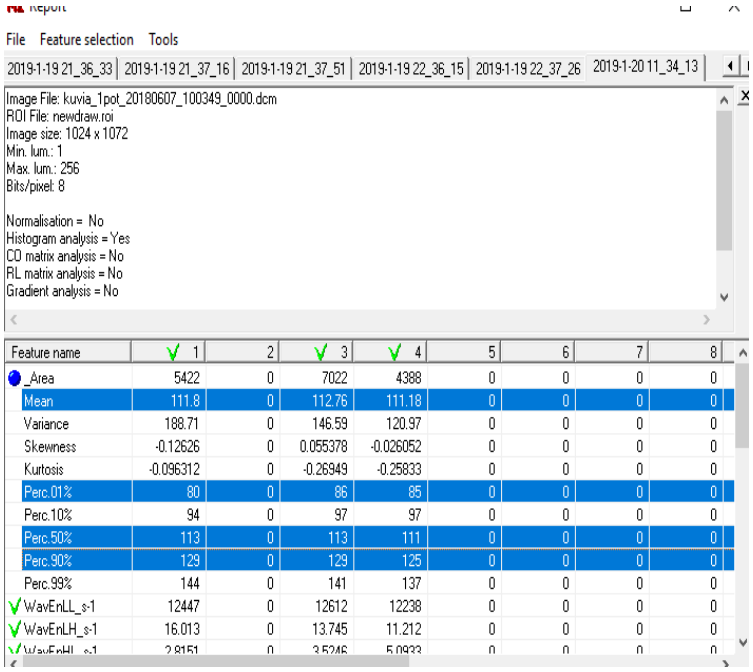

Feature name	1	2	3	4	5	6	7	8
_Area	5422	0	7022	4388	0	0	0	0
Mean	111.8	0	112.76	111.18	0	0	0	0
Variance	188.71	0	146.59	120.97	0	0	0	0
Skewness	-0.12626	0	0.055378	-0.026052	0	0	0	0
Kurtosis	-0.096312	0	-0.26949	-0.25833	0	0	0	0
Perc.01%	80	0	86	85	0	0	0	0
Perc.10%	94	0	97	97	0	0	0	0
Perc.50%	113	0	113	111	0	0	0	0
Perc.90%	129	0	129	125	0	0	0	0
Perc.99%	144	0	141	137	0	0	0	0
WavEnLL_s-1	12447	0	12612	12238	0	0	0	0
WavEnLH_s-1	16.013	0	13.745	11.212	0	0	0	0

Figure 5.1.4 *Report window for histogram based texture parameters (highlighted blue) with a very strong similarity. The variation on some of the parameters is due to the different area of ROI selection and can be cross-checked by having the same area ROI in all cases. MaZda has an option for that procedure.*

RLM based texture parameters (horizontal short run and horizontal long run). Run length based texture parameters for three ROI have similar results (highlighted blue). Figure 5.1.5 shows the report window for RLM based texture parameters.

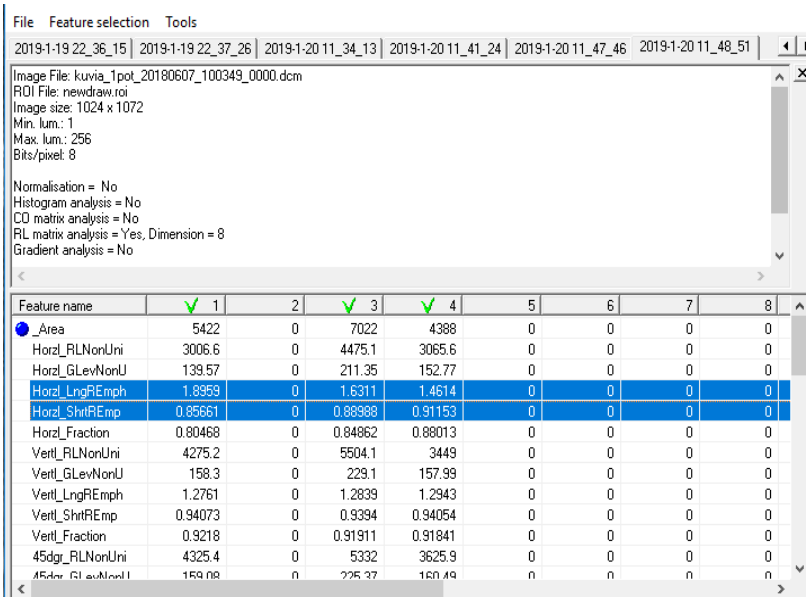

Figure 5.1.5 *Report window for RLM based texture parameters (highlighted blue) with a very strong similarity between ROI selected.*

Absolute gradient based texture parameters for the three ROIs. We can see that the parameters (highlighted blue) for the three ROI does not have significant variations. Figure 5.1.6 shows the report window for absolute gradient based texture parameters.

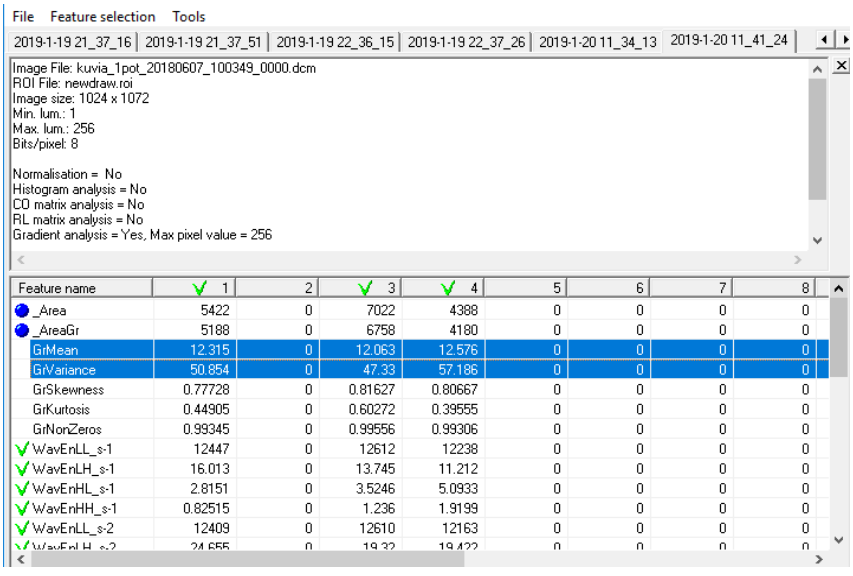

Figure 5.1.6 *Report window for gradient based texture parameters (highlighted blue) with a very strong similarity between ROIs.*

COM-based texture parameters for the three ROIs showed similar results for ROI3 and ROI1. There is a variation of contrast on ROI4 compared with the other two. The symmetric ROIs (ROI1, ROI3) have shown a strong contrast similarity as expected and the lateral ROI has shown relatively significant variation. That is partly due to its closeness

to the fibrous capsule and the higher echogenicity from the capsule interfere with the analysis making the average contrast become higher. And the other factors is the area of ROI selection as we can see the lateral ROI has a smaller area than the other ROIs means that there is a small number of the pixels in this area giving the mean contrast calculation to have a narrow range. However, all the other COM parameters have a very strong similarity. Figure 5.1.7 shows the report window for COM-based texture parameters.

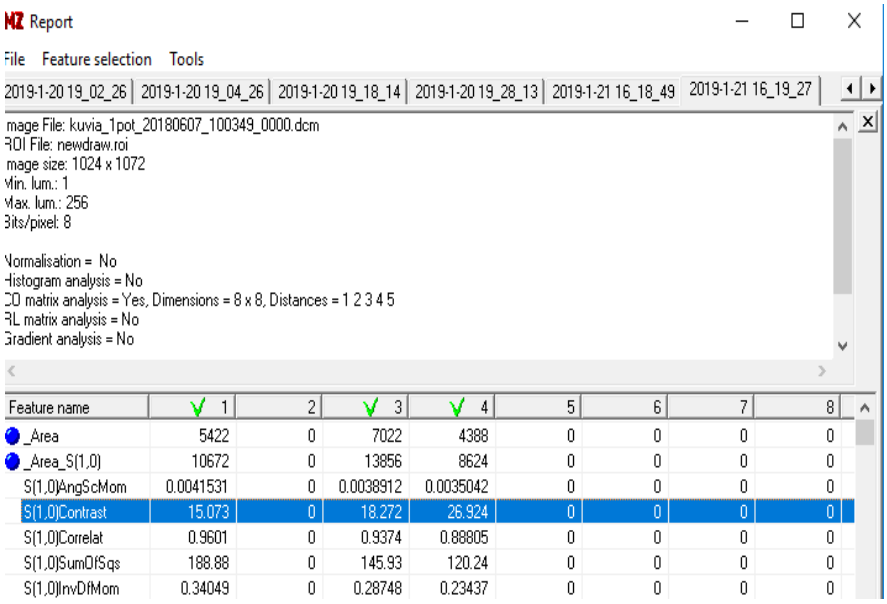

Figure 5.1.7 *Report window for COM-based texture parameters with a strong similarity of contrast (highlighted blue) between the first two ROIs but variation on the third ROI. All the other parameters have strong similarity in all ROIs.*

From these texture parameters, we can assume that the PZ has a uniform (similar) texture parameters for the selected ROI coinciding with the sonographic appearance. However, this is not very conclusive and if we want to increase the accuracy, we need to increase the number of ROI to include most or all areas of the PZ. By doing that if, we found any ROI with abnormal texture parameters from the rest of ROIs that site will be the main area of interest for biopsy extraction and further analysis giving a higher diagnostic accuracy and avoid repeat biopsy.

This method can be also used in cases when a patient has abnormal serum PSA value and positive clinical presentation but the TRUS has a normal appearance or if there is a suspicion of isoechoic or early stage pathologic echotexture on the zone.

This “normal” texture parameters results can also be used as a reference to compare the texture parameters we might get in case of pathological conditions.

However, in practice, we might not start by having this kind of extensive analysis with a large number of ROIs because it will be time consuming and has a higher probability of commuting errors.

If we analyze a confirmed, normal PZ of prostate from different age groups, we might develop mean standard texture parameters that will be used for comparison. We can select the whole PZ that we get from new patients as one ROI and compare it with the standard and if it has a strong variation from the standard, we might proceed to the detailed analysis in order to detect the abnormal area precisely. Figure 5.1.8 shows whole area of PZ as one ROI.

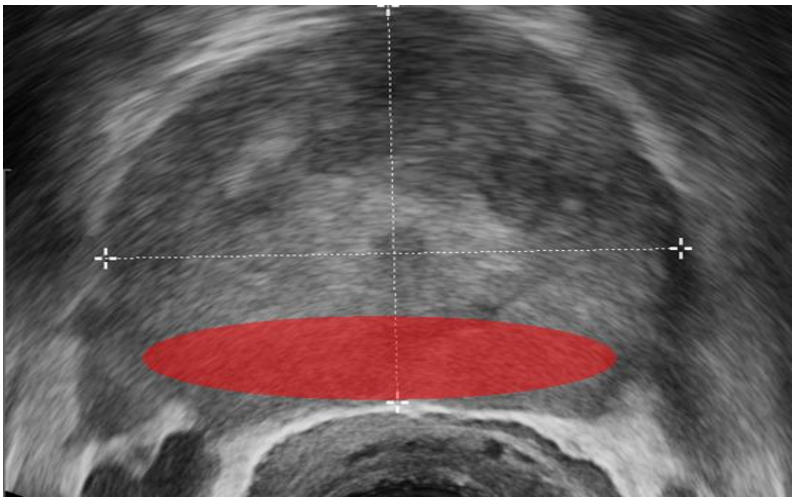

Figure 5.1.8 *Setting the whole PZ as one ROI in order to get a firsthand information about the condition of the zone by comparing it with the standard texture features developed from the confirmed normal PZ.*

If we do not have the standard and we want to save time and avoid the errors, we can set the right PZ and left PZ as single symmetric ROIs and see if they have similar texture features before proceeding. Figure 5.1.9 shows setting of the right side PZ and left side PZ as a symmetric ROI.

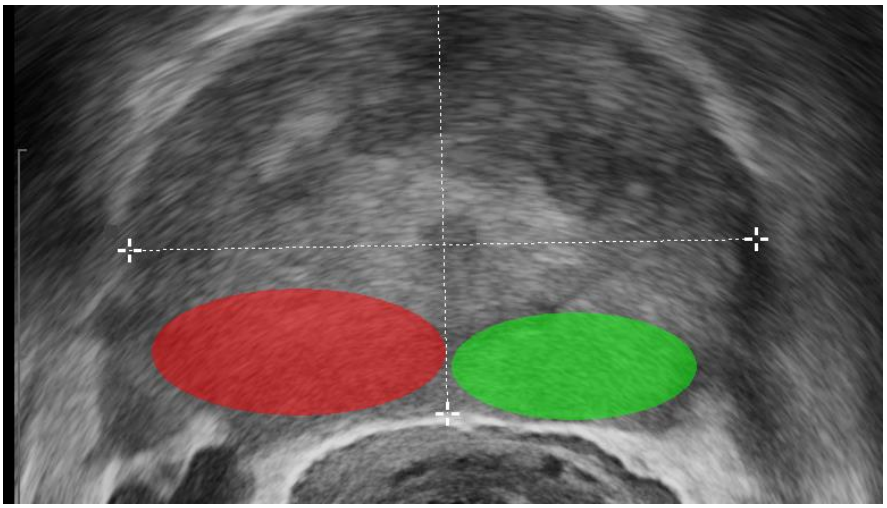

Figure 5.1.9 *Symmetric ROI selection of right and left PZ. If they show symmetric texture distribution, we can divert the focus of the analysis into the other regions of the gland.*

5.2 Texture analysis of hypoechoic areas on the PZ

For this particular analysis, we have used a random image (image 102905_0000.dcm) that showed a well-defined nodular hypoechoic area on the left lateral PZ. Figure 5.2.1 shows axial scan of prostate.

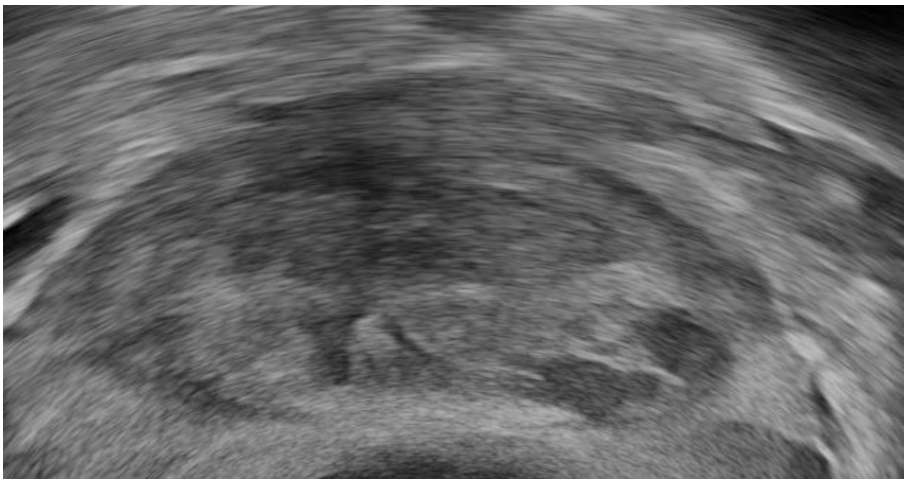

Figure 5.2.1 *Axial mid gland scan with two well-defined nodular hypoechoic areas on the left PZ.*

The intention of this analysis is to see the texture parameters between the two nodular hypoechoic areas. We have set the two nodular areas as a separate ROI using a free hand region of interest selection. Figure 5.2.2 shows ROI selection.

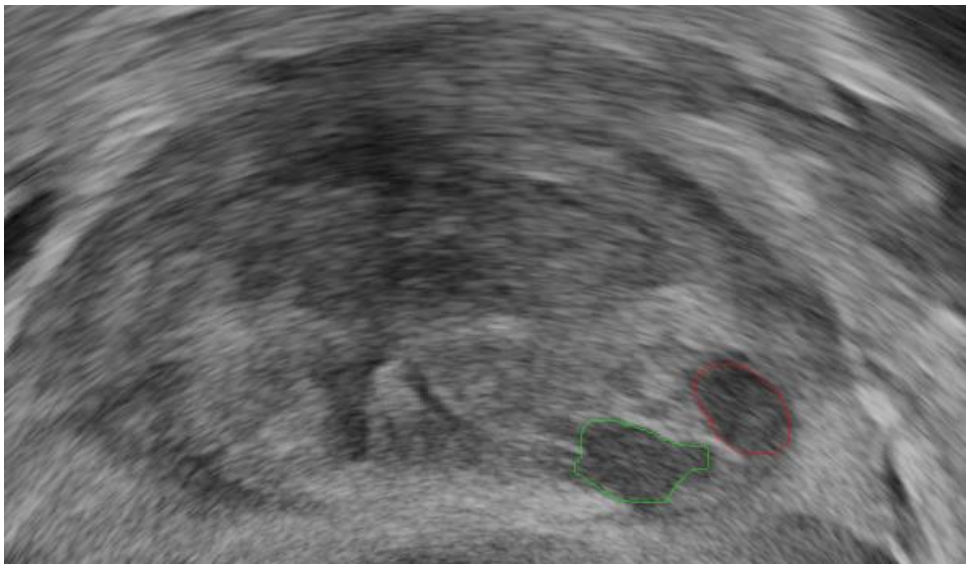

Figure 5.2.2 *Free hand ROI selection, we have used free hand selection method in order to include the full area of the nodular structures precisely.*

Histogram based texture parameters have showed a strong similarity between the maximum and minimum luminosity of the ROIs. Figure 5.2.3 histogram charts of the ROIs.

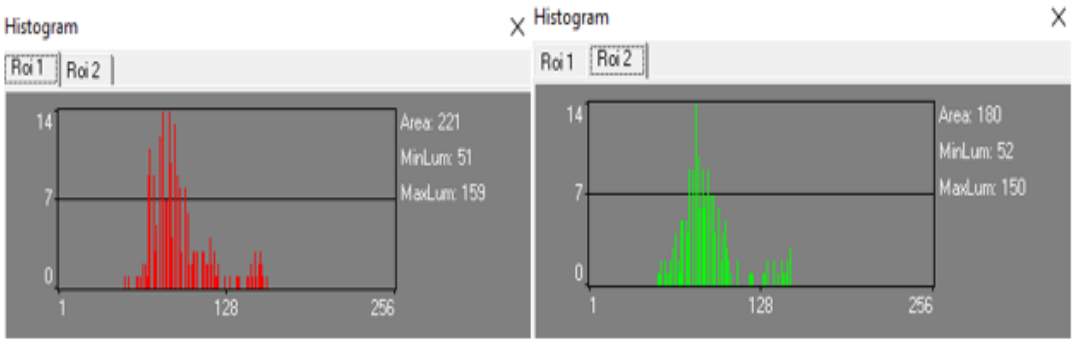

Figure *5.2.3 Histogram charts showing a very strong similarity between the average maximum and minimum gray level values of the pixels in the respective ROIs.*

We can execute the histogram report window to see the mean, variance and percentile parameters. Figure 5.2.4 shows the report window for histogram based texture parameters

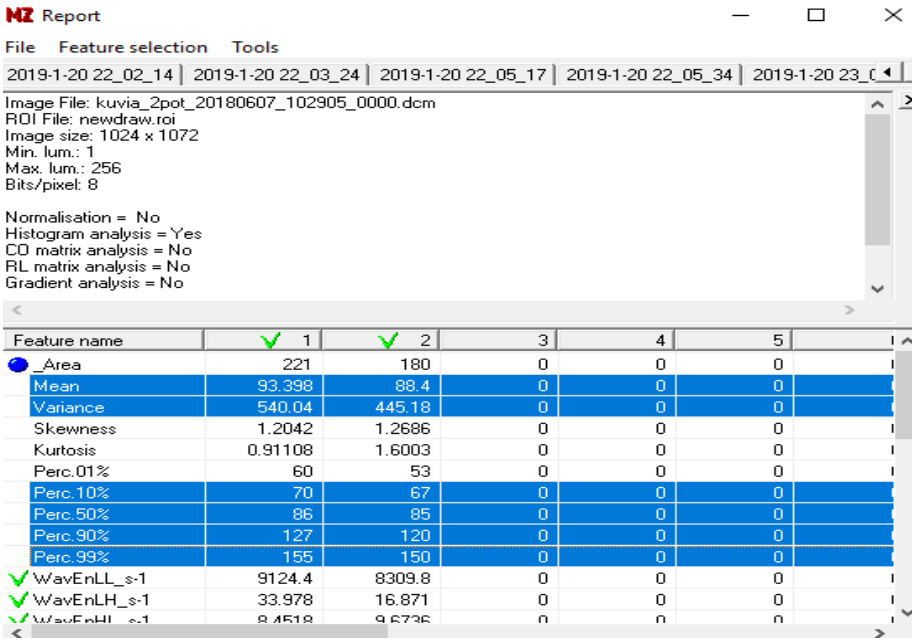

Figure 5.2.4 *Report window for histogram based texture parameters (highlighted blue) with a very strong similarity. The significant difference in the variance is created due to an unequal area of ROI selection that can be checked by setting one RIO on the first nodule and loading the same area ROI on the second nodule (selecting the same area of ROI for both).*

COM based texture parameter shows an almost same contrast and entropy between the ROIs and in all the other parameters. Figure 5.2.5 shows the report window for COM based texture parameters.

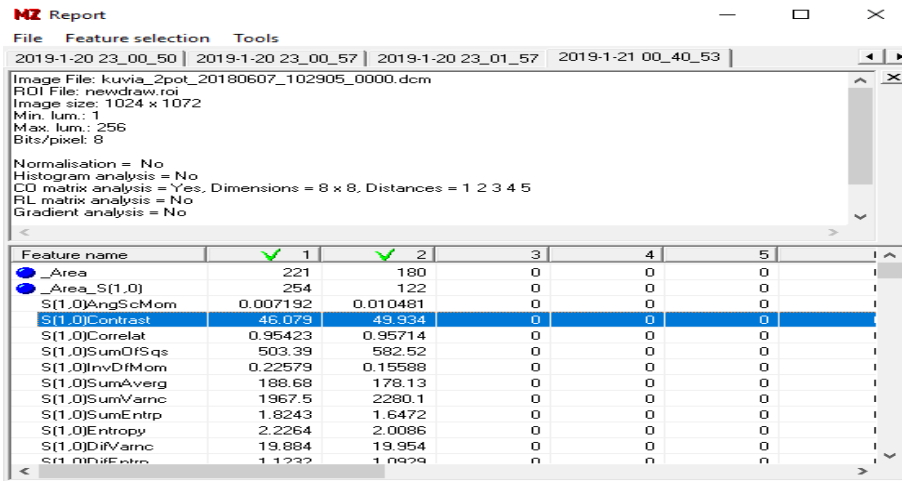

Figure 5.2.5. *Report window for the COM based texture parameters for the ROI showing a strong similarity on the contrast of the two ROI (high-lighted blue).*

Absolute gradient-based texture parameters (Gr mean and Gr variance) have same results. Figure 5.2.6 shows report window for absolute gradient-based texture parameters.

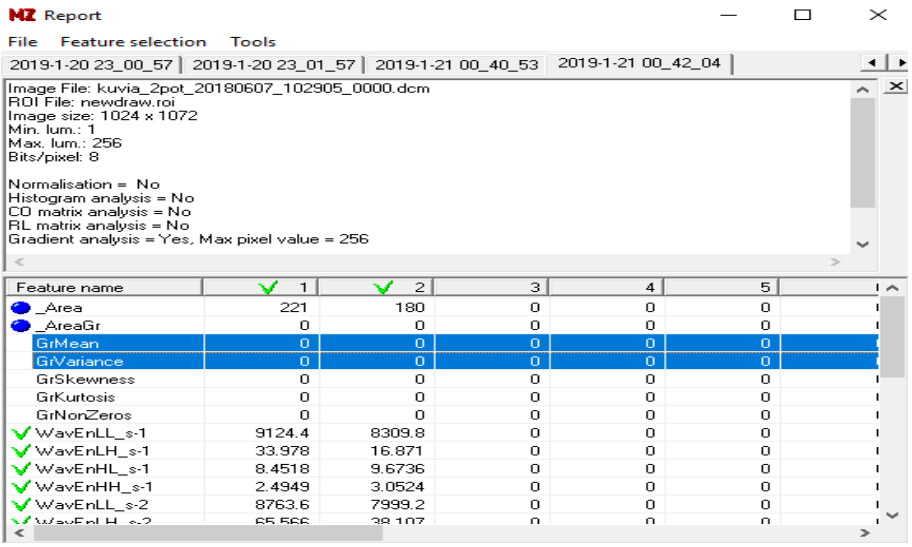

Figure 5.2.6 *Report window for absolute gradient showing the same parameters (highlighted blue) for the two ROI nodules. Mean and variance is the parameters of the absolute gradient.*

RLM based texture parameters between the two ROIs have a very strong similarity. Figure 5.2.7 shows the report window for RLM based texture parameters.

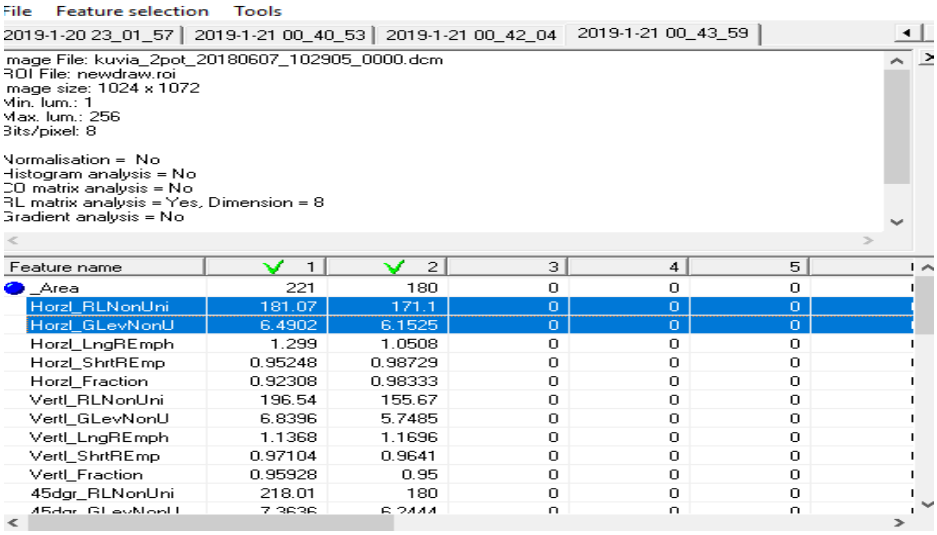

Figure 5.2.7 *Report window for run-length matrix for the RIO showing no significant variations (highlighted blue).*

The main conclusion we can make is about the underlying pathophysiologic cause of the nodules based on the similarity of the texture parameters in all cases. The final echotexture of the pathology observed is the result of the pathophysiologic pathway the disease follows. If two conditions have a different pathophysiologic route they will not have the same or similar texture parameters in all four cases. They may appear similar on sonogram but the texture parameters cannot be the same.

Therefore based on the similarity of all the statistical texture parameters for the free hand chosen two ROI we can assume that the clinical (pathophysiological) source of origin for the two hypoechoic areas is the same or similar, this will make the differential diagnosis to be narrow and more accurate. These results are based on a limited number of samples and I assume then in order to see and calculate how much accurately MaZda can evaluate the difference and similarity between two or more sonographically similar areas we need to use more samples (ROI) unlike here with only two samples.

5.3 Analyzing hypoechoic areas on the PZ from different patients

On this thesis, we have used two random scans (102858_0000.dcm and 102905_0000.dcm) that does not show significant hypertrophy (in order to minimize the chance of having the echotexture from BPH) of the gland and that have shown well-defined hypoechoic areas on the PZ and compare the texture parameters. Random ROI is chosen in both scans where hypoechoic well-defined areas are present.

By analyzing the texture parameters of multiple hypoechoic areas on the PZ of prostate from multiple scans, we might be able to produce the standard expected texture parameters of sonographically similar areas on the same zone of prostate we might encounter in the future scans from different patients. This is helpful in a way that if we see a deviation from the standard that will give us a clue about the pathological nature of the structure, this, in turn, will make the differential diagnosis more close to accuracy. Figure 5.3.1 shows axial scans of prostate from two different patients.

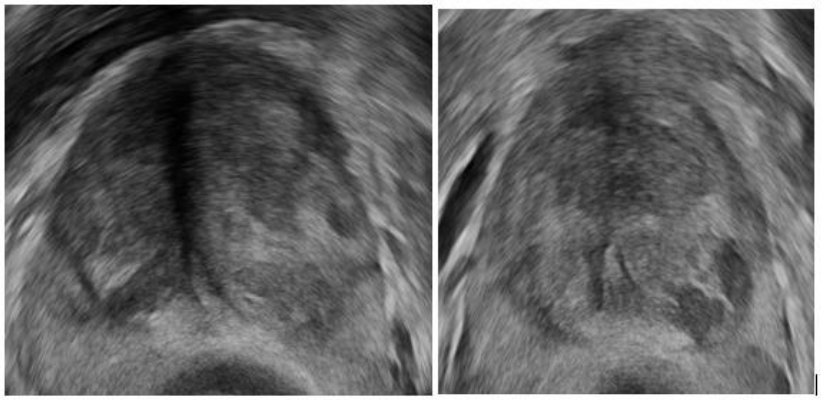

Figure 5.3.1 *Axial scan of prostate from different patients. Both sonograms shows well defined hypoechoic area on the lateral and mid PZ.*

A freehand ROI selection is used in all cases that will give us a more accurate inclusion of the area of interest. Figure 5.3.2 freehand ROI selection in both samples.

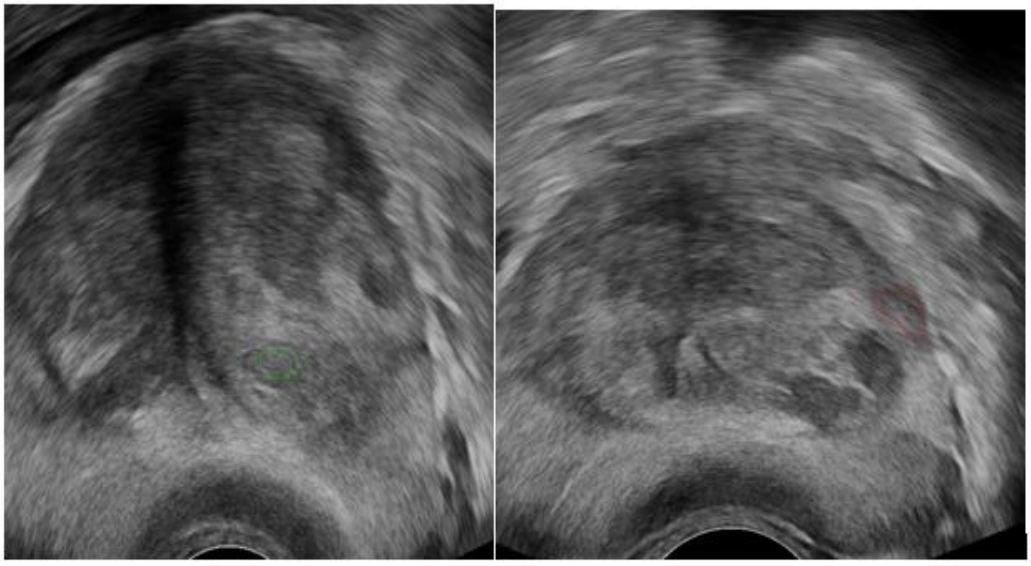

Figure 5.3.2 *Freehand ROI selection (green area) on the mid-PZ on the first scan and left lateral PZ (red area) in the second sonogram.*

Histogram-based texture parameters have shown a strong similarity between the ROIs. The average maximum and minimum gray level values of pixels in each ROI have a strong similarity. Figure 5.3.3 shows the histogram based texture parameters.

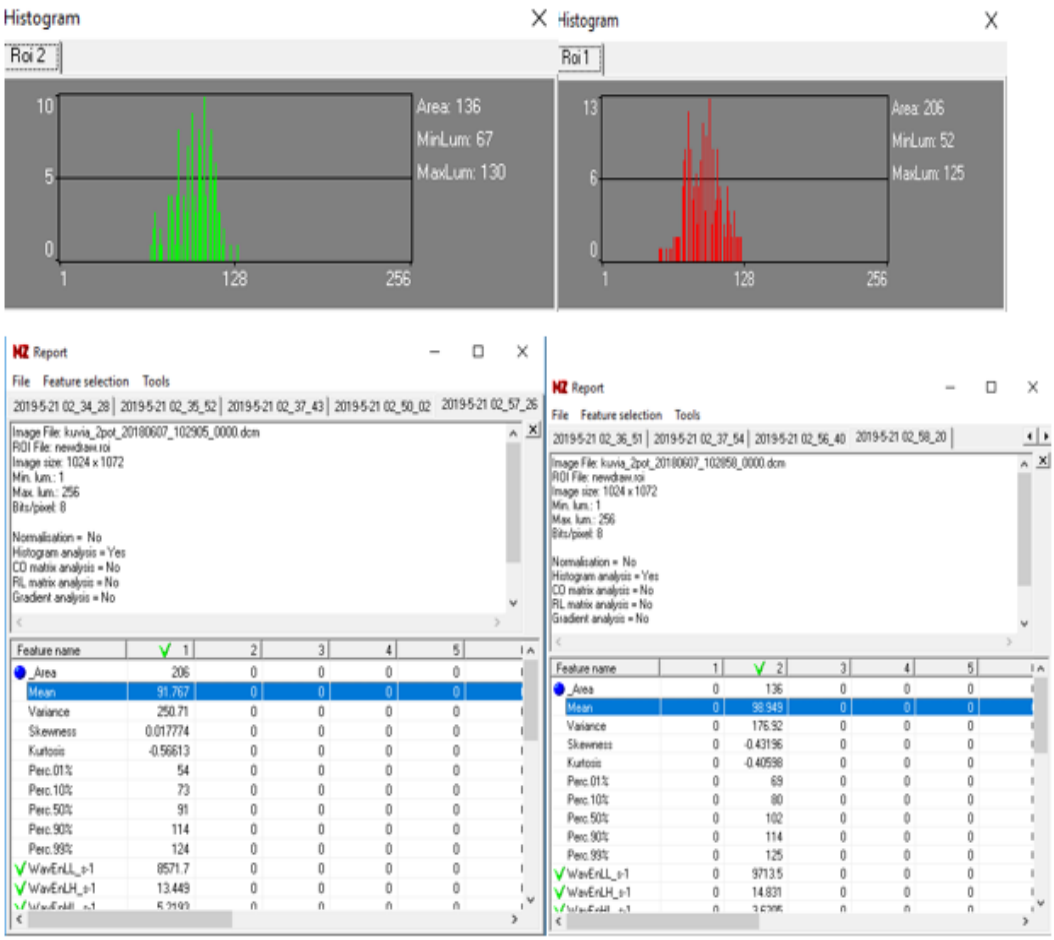

Figure 5.3.3 *Histogram charts and report window for histogram based texture parameters with a strong similarity between the pixel gray level values.*

Absolute gradient based texture parameters have strong similarity but there is a strong variation on the Grmean value. Grmean variation on the image (102905_0000.dcm) are seen on the area close to the fibrous capsule (because ROI was selected close to the capsule). It has been checked by using the standard region of interest selection that was set by avoiding the closure to the capsule and the results were found to be without significant variation (12.68). So we assume that the echogenicity of the fibrous capsule has an effect on the results. Figure 5.3.4 shows the report window for absolute gradient based texture parameters.

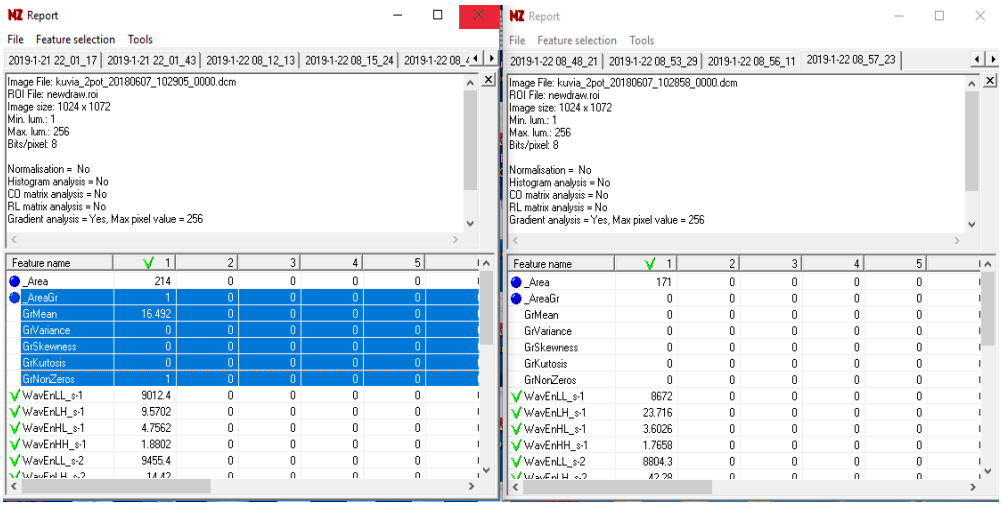

Figure 5.3.4 *Report window for the absolute gradient based texture parameters without significant variations.*

COM shows a significant difference in the contrast of the two ROI is attributed to the echogenic nature of the fibrous capsule where ROI is set close by. But the rest of the parameters doesn't show significant variation. Figure 5.3.5 shows the report window for COM-based parameters.

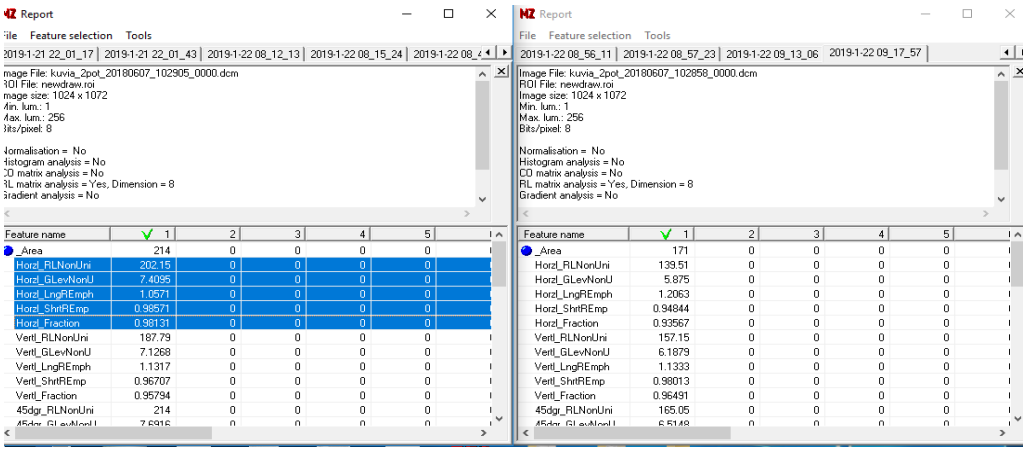

Figure 5.3.5 *Report window for COM parameters (highlighted blue) with similar results between the selected ROIs*

RLM texture parameters also show similar results. Figure 5.3.6 shows the report window for RLM based texture parameters.

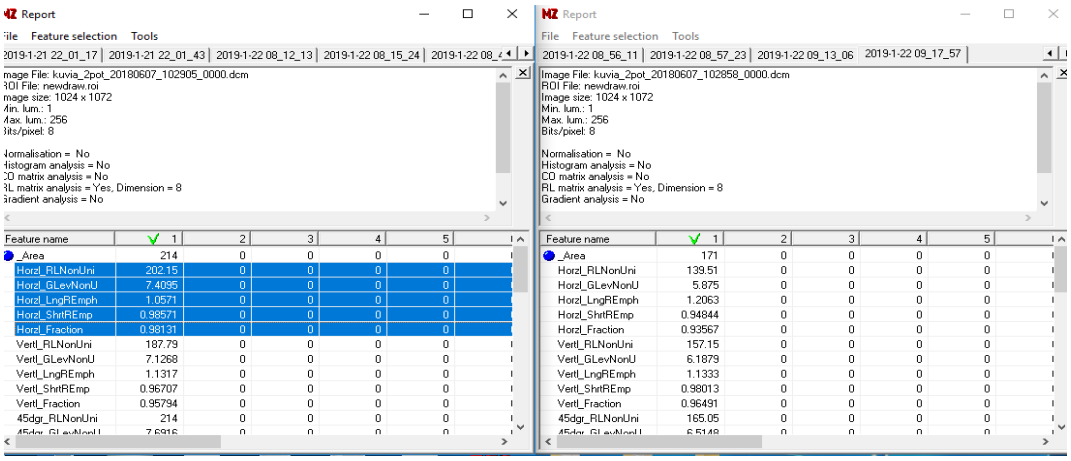

Figure 5.3.6 *report window for RLM texture parameters without significant variations between the ROIs.*

Therefore the two samples of ROI taken from the two different scans have shown a strong correlation between the texture parameters. By analyzing texture parameters from a multitude of samples we might derive the average texture feature that will be used as a standard reference point for the future analysis of structures with similar echotexture.

5.4 Analyzing hypoechoic areas outside the PZ.

Our next step is to analyze hypoechoic structures that are located outside the PZ. For this purpose, we are going to use a sonogram (with the dimensions of the gland mentioned since all the sample scans we got doesn't show the dimension of the gland) that has shown a well-defined echo poor area in the central part of the gland and knowing the age and clinical presentations would have added additional information on the suspicion of the finding. We can also compare the results with the texture parameters we have found from hypoechoic areas located on the PZ. the main objective of this analysis is to try to discriminate the PCa(mostly hypoechoic nodular appearance) that is mostly shown on the PZ and the BPH that is frequently apparent on the TZ (or central part of the gland in general) based on the texture parameters on top of the most peculiar known sonographic appearance. This will give us an added advantage to accurately differentiate the two pathologies. Figure 5.4.1 shows a sagittal scan of the prostate.

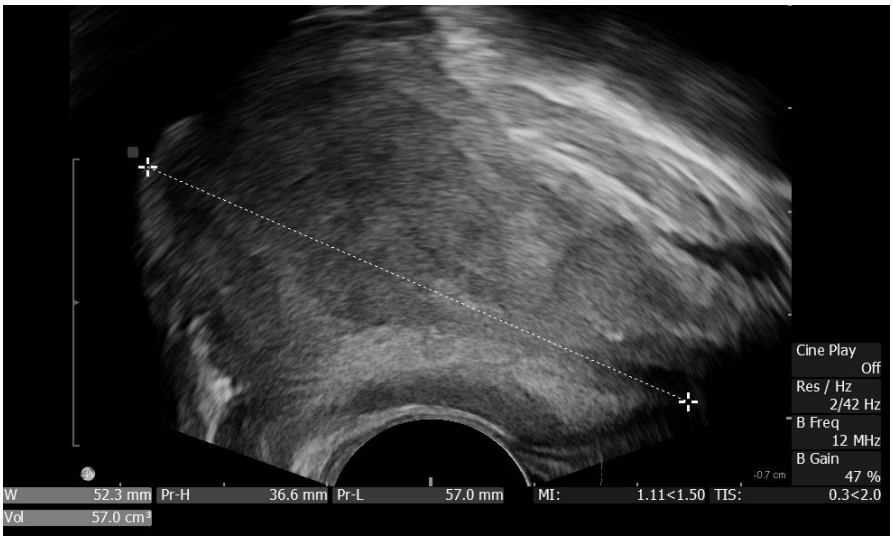

Figure 5.4.1 *Sagittal scan of the prostate. The sonogram shows significant hypertrophy of the gland (w,52.3mm, L, 57mm and V,57.0cm3), the PZ is seen reduced in thickness (mass effect from the central part of the gland might be responsible) and the central part of the gland is seen increased in thickness with well-rounded isoechoic area extending from the UB apex to the periphery of the gland.*

One first-hand comparison method of hypoechoic regions outside the peripheral zone and those in the PZ is to set a number of standard ROI on the central part of the gland and look if they have a uniform (similar results) because we have found out that those in the PZ has similar texture parameter results. We have checked the other scans on this idea but we will use only one scan here to show. Figure 5.4.2 shows ROI selection in the central part of the gland.

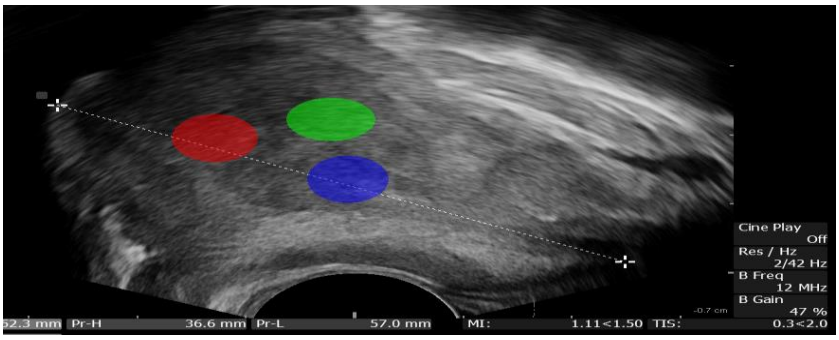

Figure 5.4.2 *Standard random ROI selection in the central part of the glnad mainly where the hypoechoic hypertrophied area is located.*

Histogram-based texture parameters have shown a strong variation between all the selected ROIs. Figure 5.4.3 shows the histogram chart and the histogram based parameters report window.

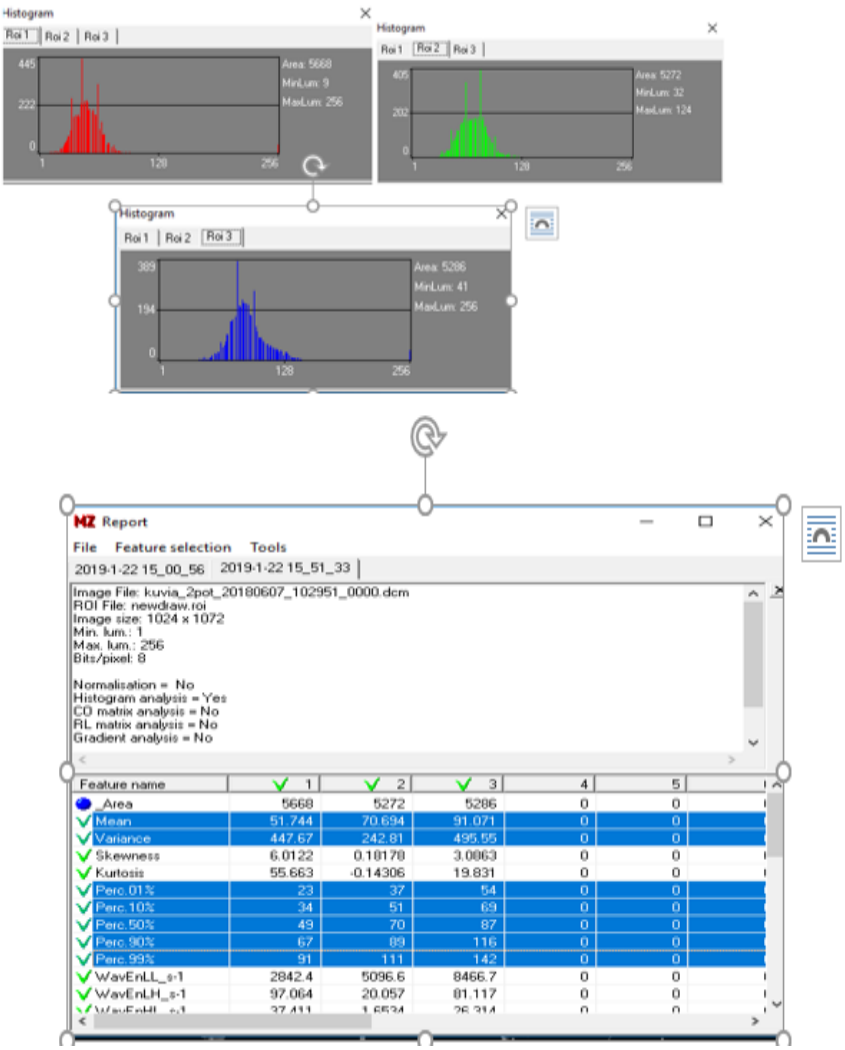

Figure 5.4.3 *Histogram chart showing a strong variation between the pixel gray level values and the report window shows strong variations on all histogram based texture parameters (highlighted blue)*

COM-based texture parameter has also shown a very strong variation in all ROIs. Figure 5.4.4 shows the report window for COM-based texture parameters.

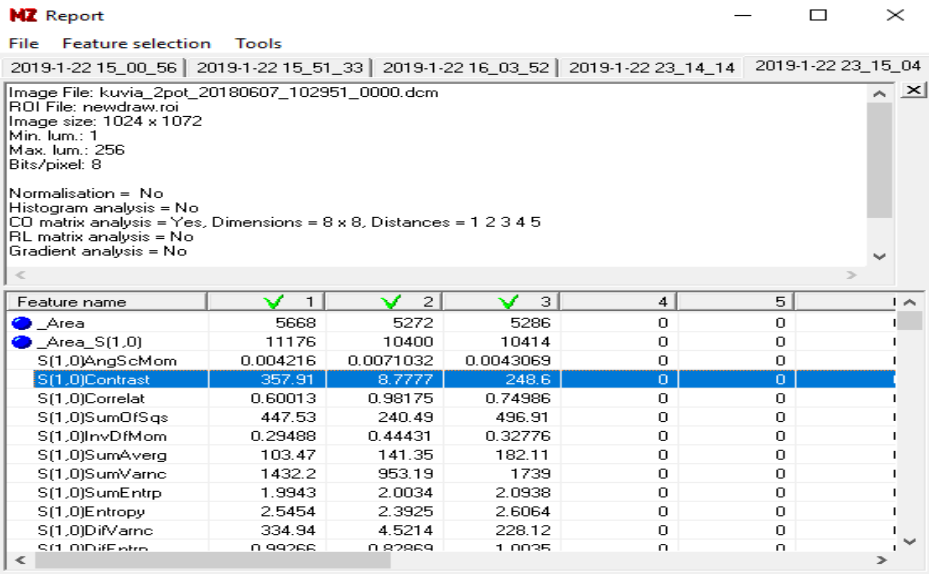

Figure 5.4.4 *Report window for COM parameter, the contrast has a very strong variation and all other parameters also show a strong variations between the ROIs.*

There is a similarity on Grmean between the ROI and significant variation on Grvariance .Figure 5.4.5 shows the report window for absolute gradient based texture parameters.

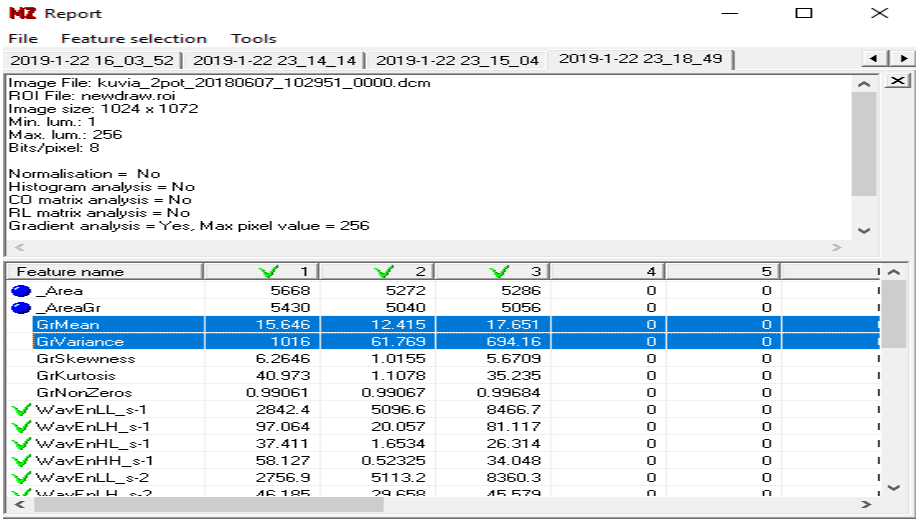

Figure 5.4.5 *Report window for absolute gradient based texture parameters with a variations in all parameters except the GrMean.*

RLM based texture parameters also have showed a strong variations between all ROIs. Figure 5.4.6 shows the report window for RLM.

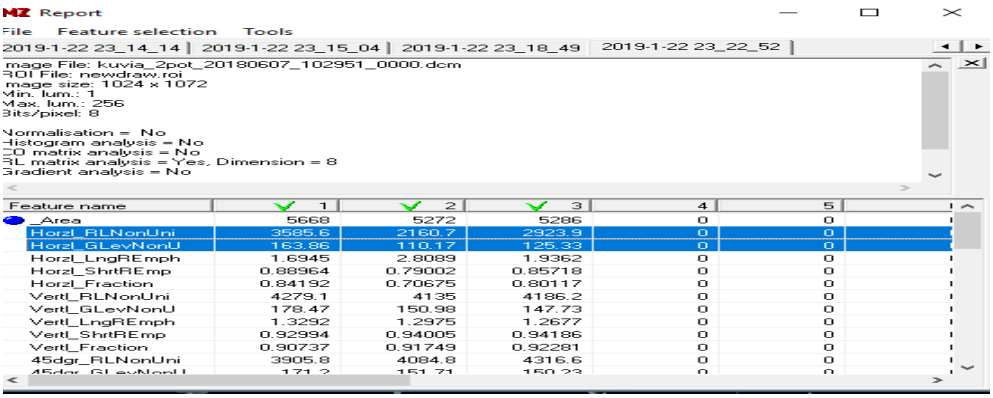

Figure *5.4.6 Report window for RLM with a significant variations of parameters(highlighted blue) between th ethree ROIs.*

We have observed that in most of the texture parameters the ROIs chosen outside the PZ have significant discrepancies that can give a clue about the underlying pathology. When we compare the results we got during our analysis of hypoechoic structures on the PZ the results were similar. all the results are based on the number of sample scans provided and we have found that all the ROI(hypoechoic areas) selected outside the PZ have a variation on the texture parameters than those found on PZ.

5.5 Analyzing hyperechoic areas

For this analysis, we are going to use a sample sonograms which shows well defined echogenic area. Image 100418_0000.dcm shows well defined echogenic structure on the mid gland. Figure 5.5.1 shows sagittal scan with well-defined echogenic nodules.

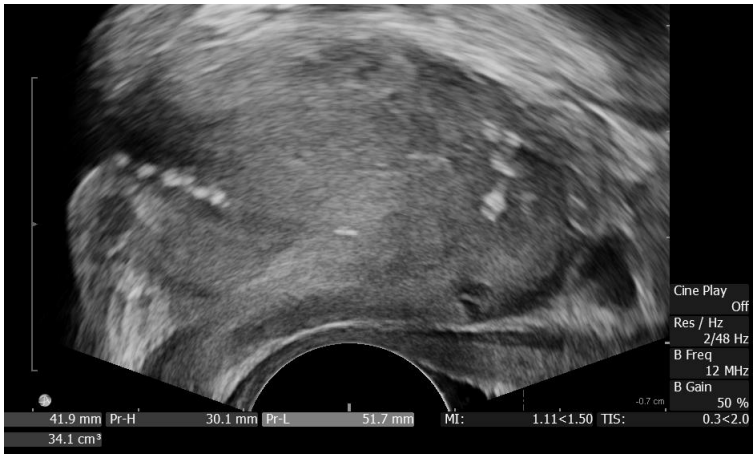

Figure 5.5.1 *Sagital scan of prostate without significant elongation. There are multiple well defined ecogenic foci bilaterally and they extend to UB that tells us that the foci are located close to the base of Prostate.*

We used a free hand ROI selection method setting all the nodular structures on the right as a single ROI and those seen on the left as another ROI. Figure 5.5.2 shows the setting of the ROI.

***Figure** 6.5.2 Sagital scan of prostate showing freehand ROI selection on the right and left aspect of the gland*

Histogram-based texture parameters have shown strong variations between the selected ROIs. Figure 5.5.2 shows the histogram charts and report for histogram parameters.

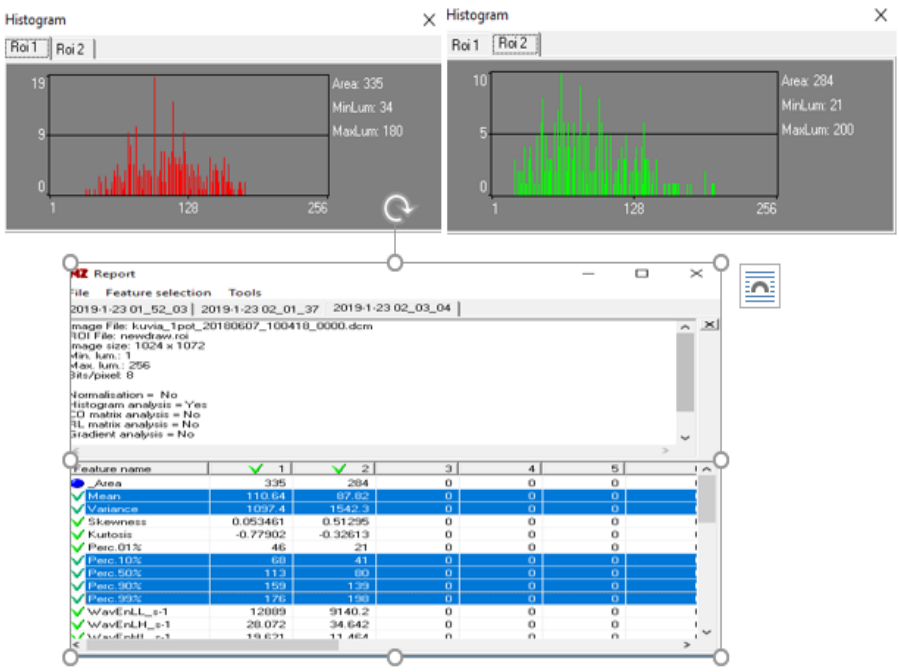

***Figure 5.5.2** Histogram charts have strong variations on the maximum and minimum luminosity of the pixels in the selected ROIs. The histogram based parameters (highlighted blue) have strong variations in all cases*

Absolute gradient based texture parameters (GrMean and GrVariance) have shown similar results (0). Figure 6.5.3 shows the report window for absolute gradient based texture parameters.

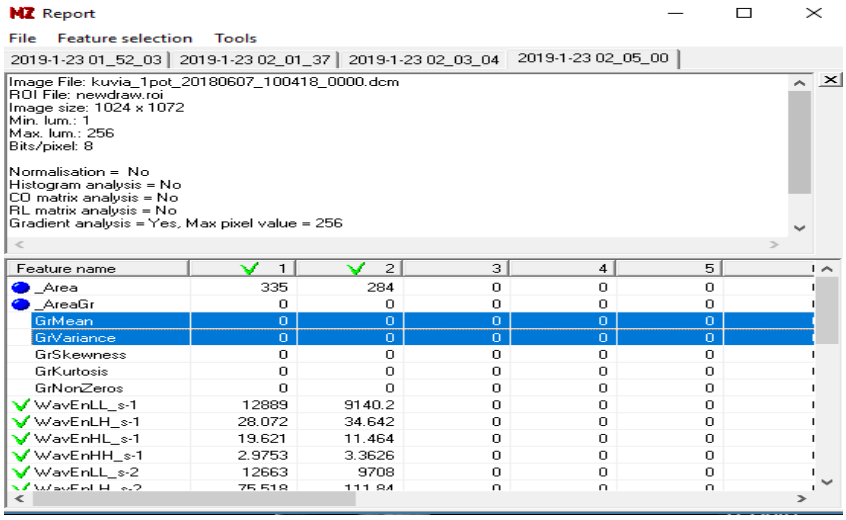

Figure 5.5.3 *Report window for absolute gradient based texture parameters showing a strong similarity between parameters (Grmean,Grvariance).*

COM-based texture parameters (contrast and entropy) have shown a strong similarity in the contrast of the ROI selected. The randomness of the pixel gray level values is similar in both ROIs but the contrast has a variation in regions where nodular structures are not located but it was included together as an ROI with the area that includes the significant hyperechoic nodules. Figure 5.5.4 shows the COM report window

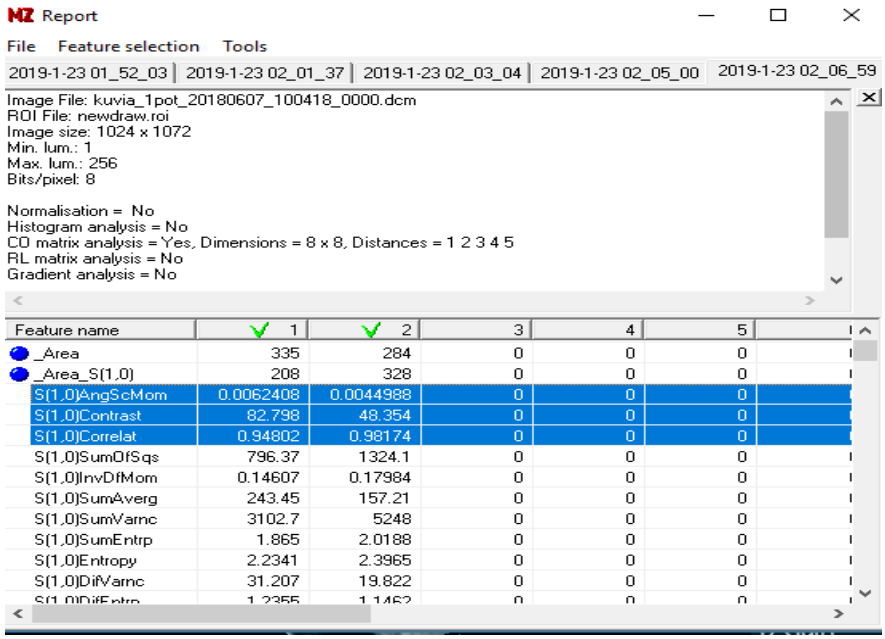

Figure 5.5.4 *Report window for COM-based texture parameters (highlighted blue).*

RLM based texture parameters have shown a strong similarity between the ROIs. Figure 5.5.6 shows the report window for RLM.

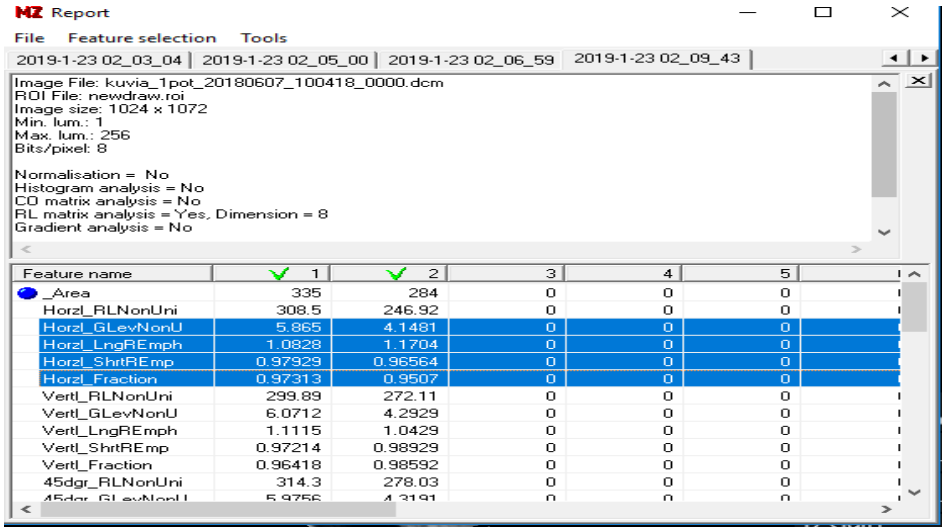

Figure 5.5.5 *Report window for RLM parameters (highlighted blue) showing strong similarity.*

In conclusion, we have a similarity of texture parameters in case of RLM and COM-based texture parameters. this analysis is affected by the area of selection that involves a non-hyperechoic area in between the nodules. In order to check the results, we need to select each nodule separately as a single ROI in order to avoid an area in between the focis and compare it with the results we obtain.

For demonstration purpose, we have set 2ROIs on the left and 2ROIs on the right side of the prostate where the hyperechoic nodules are located. Figure 5.5.6 shows ROIs selected on the right and left side.

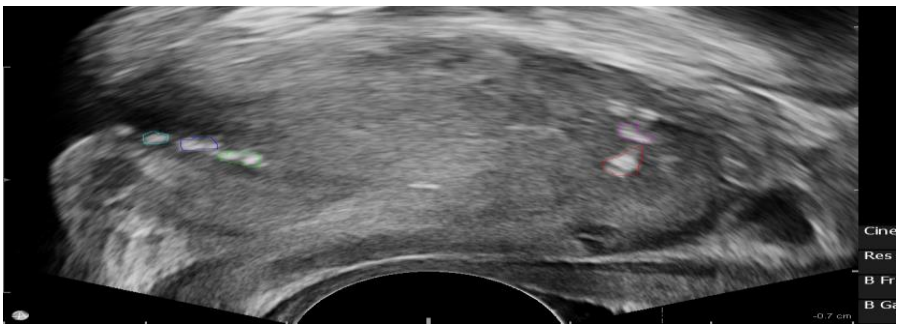

Figure 5.5.6 *Increased number of ROI selection that only involves hyperechoic areas.*

Histogram-based texture parameters have shown a strong variations in all parameters that agrees with the first method of analysis. We have checked all the other parameters and there is no similarity in any of parameters. Figure 5.5.6 shows the histogram charts for each ROIs.

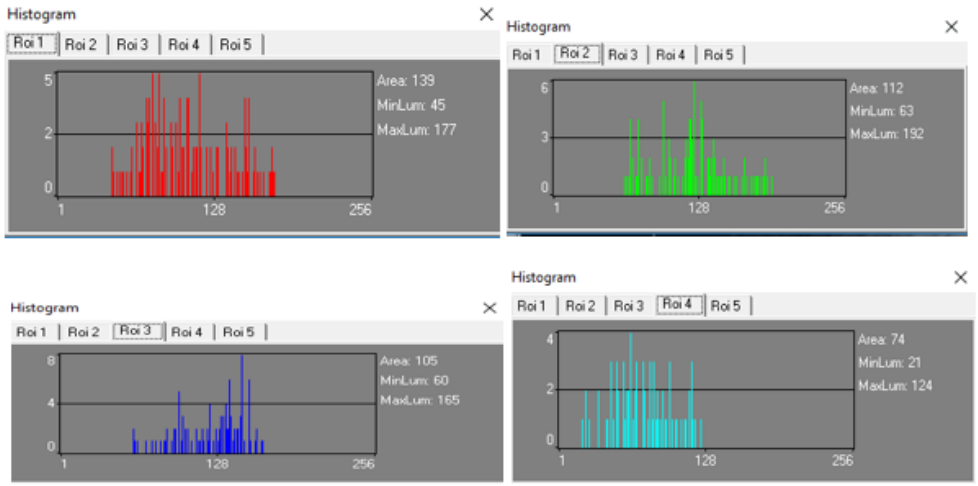

Figure 5.5.7 *Histogram charts for each ROI. Even though they all look hyperechoic the maximum and minimum luminosity has very strong variations.*

We can make the histogram map of the image in order to filter out the foci particularly. Figure 5.5.7 shows the histogram map of the image.

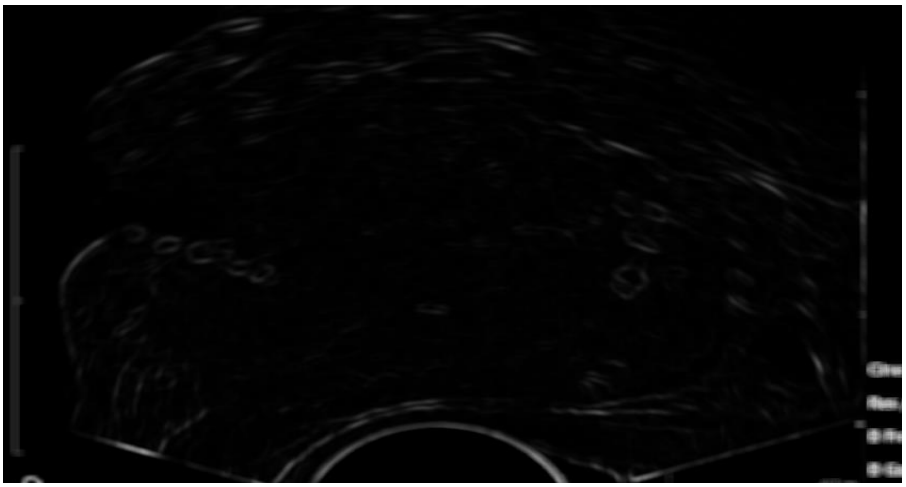

Figure 5.5.8 *Histogram map of the same scan showing multiple well rounded echogenic nodules on both sides of the prostate. There is no significant echogenic structure on the rest of the gland volume.*

In general, for any type of abnormal echotexture, some parameters showed a strong similarity than the other. In order to identify these parameters and use them as a standard reference point a large number of samples that are pre-confirmed may need to be evaluated in each particular case.

The variations between the standard and freehand methods of ROI selection have to be considered when we compare the results between two or more areas. Superimposed ROI selection may give more accurate results and that might as well be used for cross-checking purpose with the results we get by using a free hand or standard ROI selection. We can also use a polygonal method for ROI selection if we precisely have to include the full area of interest especially those that have an irregular border. The line thickness of the ROI selection has to be considered also when setting an ROI between two areas that have a significant difference in echogenicity and during superimposed ROI selection or when setting ROI very close to each other that there is a cross-link between the outer borders of the ROIs at one or more points.

6. DISCUSSION AND CONCLUSION

The main intention of this thesis work is to investigate in general if we can determine one or more peculiar texture parameters for a given pathologic condition and PCa in particular by using MaZda. We have seen strong texture parameters similarity of hypoechoic areas on the PZ of prostate obtained from different patients this in turn might lead us to formulating one standard texture parameters that will describe similar echo signal areas obtained in the future. As a conclusion, MaZda seems to be highly sensitive to differentiate the texture features of normal parenchyma and abnormal tissue structures with a significant variation.

We have also shown that we can determine one or more parameter similarity of texture features from different scans (different patients) that have a similar echo appearance. MaZda has shown to give results which are in accordance with the analysis at the cellular level. On previous studies, MaZda has shown it has the capability to differentiate normal cellular structures from the abnormal cellular structures with higher certainty [53]. This will give us a clue that since our analysis was conducted at the organ level we can reach more accurate results by starting our analysis from the cellular level by analysing PCa cell images and comparing the results with the organ level analysis outputs.

During previous studies conducted at organ level using MRI images similar method of procedure is conducted, both standard ROI and freehand ROI selection are used [53]. Freehand ROI selection is suitable especially when we have an ROI that has an irregular shape and ill-defined border than a condition that is well defined and have a regular contour. Comparison or cross-checking of results from both standard and freehand ROI can be made by using superimposed ROI and polygonal ROI selection if we want to be highly certain about the results.

No texture analysis of prostate ultrasound images have been published this far. Recently, Sidhu et al. [54] reported texture parameters of a functional MRI image in order to detect TZ tumour. The whole TZ was set as a single ROI and comparison of parameters were done by including and excluding an area on the TZ that contains a significant tumour and the results were shown a significant variation [54]. For the ROI that contains histologically significant area the kurtosis was found to be -0.05 from T1 image, entropy was 5.37 and skewness was found to be 0.08 [54]. During our analysis of US PCa images (well defined hypoechoic areas on the PZ), the skewness was 1.26, kurtosis was on average 1 and entropy was close to 2. The differences arise naturally from the completely different image information when using different imaging Modalities. We have also shown that by making a detailed analysis involving the whole region of the gland with a higher number of ROI selection it is possible to detect and locate abnormal conditions that we cannot be able to discern on US visually whether due to isoechoic nature or early prognosis of the pathology. It is also possible to differentiate the most common non-malignant conditions that show similar echo appearance with the PCa based on texture features with a significant variation. At this point, we can increase only the diagnostic accuracy of any pathologic conditions and determine if a given tissue has been infiltrated by a single or

superimposed condition without accurately determining the pathology. By starting to analyse the texture features of a confirmed pathologic condition and formulating a standard reference texture features that have a higher mean accuracy we might in the future be able to improve the level of diagnosis by applying texture analysis to US images of the prostate.

7. REFERENCES

[1] R.P. Singh, S. Gupta, U.R. Acharya, Segmentation of prostate contours for automated diagnosis using ultrasound images: A survey, Journal of Computational Science, Vol. 21, 2017, pp. 223-231. https://www.sciencedirect.com/science/article/pii/S1877750317304611.

[2] K.H. Hammerich, G.E. Ayala, T.M. Wheeler, Anatomy of the prostate gland and surgical pathology of prostate cancer, in: Anonymous (ed.), Prostate Cancer, Cambridge University Press, Cambridge, 2008, pp. 1-14.

[3] Applications of transrectal ultrasound in prostate cancer, in: The British journal of radiology, The British Institute of Radiology, England, 2012, pp. S17.

[4] S.W. Fine, V.E. Reuter, Anatomy of the prostate revisited: implications for prostate biopsy and zonal origins of prostate cancer, Histopathology, Vol. 60, Iss. 1, 2012, pp. 142-152. https://onlinelibrary.wiley.com/doi/abs/10.1111/j.1365-2559.2011.04004.x.

[5] C. Pezaro, H.H. Woo, I.D. Davis, Prostate cancer: measuring PSA, Internal Medicine Journal, Vol. 44, Iss. 5, 2014, pp. 433-440. https://onlinelibrary.wiley.com/doi/abs/10.1111/imj.12407.

[6] C.J. Harvey, J. Pilcher, J. Richenberg, U. Patel, F. Frauscher, Applications of transrectal ultrasound in prostate cancer, The British journal of radiology, Vol. 85 Spec No 1, Iss. special_issue_1, 2012, pp. S17. https://www.ncbi.nlm.nih.gov/pubmed/22844031.

[7] G. Castellano, L. Bonilha, L.M. Li, F. Cendes, Texture analysis of medical images, Clinical Radiology, Vol. 59, Iss. 12, 2004, pp. 1061-1069. https://www.sciencedirect.com/science/article/pii/S000992600400265X.

[8] Szczypiński, Piotr M.|Strzelecki, Michał|Materka, Andrzej|Klepaczko, Artur, MaZda—A software package for image texture analysis, Computer Methods and Programs in Biomedicine, Vol. 94, Iss. 1, 2008, pp. 66-76. https://www.clinicalkey.es/playcontent/1-s2.0-S0169260708002083.

[9] Anatomic Imaging of the Prostate, in: BioMed Research International, Hindawi Limited, New York, 2014, pp. 728539-9.

[10] P.H. Walz, H. Bertermann, Ultrasound Examination of Bladder and Prostate, Urologia Internationalis, Vol. 45, Iss. 4, 1990, pp. 217-230. https://www.karger.com/Article/FullText/281712.

[11] C. Kim, J. Cho, Introduction, in: Anonymous (ed.), Radiology Illustrated: Uroradiology, Springer Berlin Heidelberg, Berlin, Heidelberg, 2012, pp. 825-833.

[12] K.H. Hammerich, G.E. Ayala, T.M. Wheeler, Anatomy of the prostate gland and surgical pathology of prostate cancer, in: Anonymous (ed.), Prostate Cancer, Cambridge University Press, Cambridge, 2008, pp. 1-14.

[13] F.H. Netter MD, Pelvis and Perineum, in: Anonymous (ed.), Atlas of Human Anatomy, Seventh Edition ed., 2019, pp. 441.e11.

[14] Review of Prostate Anatomy and Embryology and the Etiology of BPH, 2016, .

[15] Aaron, LaTayia, BS|Franco, Omar E., MD, PhD|Hayward, Simon W., PhD, Review of Prostate Anatomy and Embryology and the Etiology of Benign Prostatic Hyperplasia, Urologic Clinics of North America, Vol. 43, Iss. 3, 2016, pp. 279-288. https://www.clinicalkey.es/playcontent/1-s2.0-S0094014316300131.

[16] T. Bilhim, J. Pisco, A. Furtado, D. Casal, D. Pais, L. Pinheiro, J. O'Neill, Prostatic arterial supply: demonstration by multirow detector Angio CT and Catheter Angiography, European Radiology, Vol. 21, Iss. 5, 2011, pp. 1119-1126. https://www.ncbi.nlm.nih.gov/pubmed/21116632.

[17] A. Kumar, M. Sharma, Basics of Human Andrology : A Textbook, Springer Singapore Pte. Limited, Singapore, 2017, .

[18] Basics of Human Andrology, Springer Singapore, Singapore, 2017, .

[19] A.K. Tewari, P. Whelan, J.D. Graham, Understanding the Histopathology, in: Anonymous (ed.), Prostate Cancer, John Wiley & Sons, Ltd, Chichester, UK, 2014, pp. 34-48.

[20] A.K. Tewari, Prostate cancer, Wiley-Blackwell, Chichester, 2014, .

[21] B. Pullar Nimish, surgery, prostate cancer, Vol. 2016, Iss. 10, 2016, pp. 505-511.

[22] R.A. Castillejos-Molina, F.B. Gabilondo-Navarro, Salud publica de Mexico, prostate cancer, Vol. 58, Iss. 2, 2016, pp. 279-284.

[23] F. Algaba, I. Trias, Y. Arce, Natural history of prostatic carcinoma: the pathologist's perspective, Recent results in cancer research. Fortschritte der Krebsforschung. Progres dans les recherches sur le cancer, Vol. 175, 2007, pp. 9. https://www.ncbi.nlm.nih.gov/pubmed/17432551.

[24] Histopathology and Molecular Biology of Prostate Atrophy, in: Anonymous (ed.), Prostate Cancer, Humana Press, Totowa, NJ, 2008, pp. 1-15.

[25] E.A. Klein, Prostate Carcinoma: Introduction, in: Anonymous (ed.), Imaging in Oncological Urology, Springer London, London, 2009, pp. 211-219.

[26] J.C. Klink, R. Miocinovic, C. Magi Galluzzi, E.A. Klein, High-Grade Prostatic Intraepithelial Neoplasia, Korean Journal of Urology, Vol. 53, Iss. 5, 2012, pp. 297-303.

http://synapse.ko-reamed.org/search.php?where=aview&id=10.4111/kju.2012.53.5.297&code=0020KJU&vmode=FULL.

[27] D.K. Price, Androgens and Prostate Cancer in: Douglas. K Price, Ann W. Hsing (ed.), Drug Management of Prostate Cancer, Springer New York, 2010, pp. 53-59.

[28] N. Weigel, Androgen Receptor Coactivators and Prostate Cancer, in: Anonymous (ed.), Hormonal Carcinogenesis V, Springer New York, New York, NY, 2008, pp. 245-255.

[29] C. Kim, J. Cho, Introduction, in: Anonymous (ed.), Radiology Illustrated: Uroradiology, Springer Berlin Heidelberg, Berlin, Heidelberg, 2012, pp. 825-833.

[30] A.E. Powles, D.J. Martin, I.T. Wells, C.R. Goodwin, Physics of ultrasound, Anaesthesia & Intensive Care Medicine, Vol. 19, Iss. 4, 2018, pp. 202-205. https://www.sciencedirect.com/science/article/pii/S1472029918300171.

[31] D. Williams, The physics of ultrasound, Anaesthesia and Intensive Care Medicine, Vol. 13, Iss. 6, 2012, pp. 264-268. https://www.clinicalkey.es/playcontent/1-s2.0-S1472029912000756.

[32] D. Lieu, Ultrasound physics and instrumentation for pathologists, Archives of pathology & laboratory medicine, Vol. 134, Iss. 10, 2010, pp. 1541. https://www.ncbi.nlm.nih.gov/pubmed/20923312.

[33] Thorsen, Amy J., MD|Lakin, Gaio E., PhD, Basic Physics of Ultrasonography, Seminars in Colon and Rectal Surgery, Vol. 21, Iss. 4, 2010, pp. 186-190. https://www.clinicalkey.es/playcontent/1-s2.0-S1043148910000734.

[34] D. Feller-Kopman, Physics and Principles of Ultrasound Imaging, in: Anonymous (ed.), Endobronchial Ultrasound, Springer US, New York, NY, 2009, pp. 1-11.

[35] P.R. Hoskins, K. Martin, A. Thrush, Diagnostic ultrasound, 2. ed. ed. Cambridge University Press, Cambridge, UK, 2010, .

[36] Szczypiński, Piotr M.|Strzelecki, Michał|Materka, Andrzej|Klepaczko, Artur, MaZda—A software package for image texture analysis, Computer Methods and Programs in Biomedicine, Vol. 94, Iss. 1, 2008, pp. 66-76. https://www.clinicalkey.es/playcontent/1-s2.0-S0169260708002083.

[37] G. Castellano, L. Bonilha, L.M. Li, F. Cendes, Texture analysis of medical images, Clinical Radiology, Vol. 59, Iss. 12, 2004, pp. 1061-1069. https://www.sciencedirect.com/science/article/pii/S000992600400265X.

[38] Szczypiński, Piotr M.|Strzelecki, Michał|Materka, Andrzej|Klepaczko, Artur, MaZda—A software package for image texture analysis, Computer Methods and Programs in Biomedicine, Vol. 94, Iss. 1, 2008, pp. 66-76. https://www.clinicalkey.es/playcontent/1-s2.0-S0169260708002083.

[39] L. Nogueira, R. Corradi, J.A. Eastham, Prostatic specific antigen for prostate cancer detection, International braz j urol, Vol. 35, Iss. 5, 2009, pp. 521-531. https://doaj.org/article/4799343835af487f9a6f6a3cbded5f78.

[40] DAVID C.MILLER, DAVID K.ORNSTEIN, GERALS L.ANDRIOLE, SCREENNING FOR PROSTATE CANCER: an overview
, in: M.I. Resnick, I.M. Thompson (ed.), Advanced Therapy of Prostate Disease, B. C. Decker Incorporated, 2000, pp. 50-60.

[41] Stacy LoebMisop HanWilliam J. Catalona, Prostate-Specific Antigen and Prostate Cancer Screening, in: Anonymous (ed.), Prostate Biopsy: Indications, Techniques, and Complications, Humana Press, 2008, pp. 15-27.

[42] B.K. Park, Ultrasound-guided genitourinary interventions: principles and techniques, Ultrasonography (Seoul, Korea), Vol. 36, Iss. 4, 2017, pp. 336-348. https://www.ncbi.nlm.nih.gov/pubmed/28736429.

[43] Hong, Cheng William, BS|Amalou, Hayet, MD|Xu, Sheng, PhD|Turkbey, Baris, MD|Yan, Pingkun, PhD|Kruecker, Jochen, PhD|Pinto, Peter A., MD|Choyke, Peter L., MD|Wood, Bradford J., MD, Prostate Biopsy for the Interventional Radiologist, Journal of Vascular and Interventional Radiology, Vol. 25, Iss. 5, 2014, pp. 675-684. https://www.clinicalkey.es/playcontent/1-s2.0-S1051044313023506.

[44] M. Mitterberger, Prostate Carcinoma: Conventional Imaging Techniques – Gray-Scale, Color, and Power Doppler Ultrasound, in: Anonymous (ed.), Imaging in Oncological Urology, Springer London, London, 2009, pp. 221-228.

[45] Real-time balloon inflation elastography for prostate cancer detection and initial evaluation of clinicopathologic analysis, in: AJR. American journal of roentgenology, United States, 2010, pp. W476.

[46] M. Mitterberger, W. Horninger, F. Aigner, G.M. Pinggera, I. Steppan, P. Rehder, F. Frauscher, Ultrasound of the prostate, Cancer imaging : the official publication of the International Cancer Imaging Society, Vol. 10, Iss. 1, 2010, pp. 40-48. https://www.ncbi.nlm.nih.gov/pubmed/20199941.

[47] C.J. Harvey, J. Pilcher, J. Richenberg, U. Patel, F. Frauscher, Applications of transrectal ultrasound in prostate cancer, The British journal of radiology, Vol. 85 Spec No 1, Iss. special_issue_1, 2012, pp. S17. https://www.ncbi.nlm.nih.gov/pubmed/22844031.

[48] Ultrasound of the prostate, in: Cancer imaging : the official publication of the International Cancer Imaging Society, e-Med, England, 2010, pp. 40-48.

[49] P.L. Choyke, P.A. Pinto, B. Turkbey, Imaging techniques for prostate cancer: implications for focal therapy, Nature Reviews Urology, Vol. 6, Iss. 4, 2009, pp. 191-203. http://dx.doi.org/10.1038/nrurol.2009.27.

[50] S. Kim, M. Moon, B. Park, Clinical Applications of Transrectal Ultrasound in the Prostate and Seminal Tract, Journal of Medical Ultrasound, Vol. 10, Iss. 4, 2002, pp. 181-190. https://www.sciencedirect.com/science/article/pii/S0929644109600345.

[51] A. H. Hou, D. Swanson, A. B. Barqawi, Modalities for Imaging of Prostate Cancer, Advances in urology, Vol. 2009, 2009, pp. 818065-12. http://dx.doi.org/10.1155/2009/818065.

[52] S. Kim, M. Moon, B. Park, Clinical Applications of Transrectal Ultrasound in the Prostate and Seminal Tract, Journal of Medical Ultrasound, Vol. 10, Iss. 4, 2002, pp. 181-190. https://www.sciencedirect.com/science/article/pii/S0929644109600345.

[53] HARRISON, L. (2011). *clinical applicability of MRI texture analysis*. Ph.D. university of tampere.

[54] Sidhu, H., Benigno, S., Ganeshan, B., Dikaios, N., Johnston, E., Allen, C., Kirkham, A., Groves, A., Ahmed, H., Emberton, M., Taylor, S., Halligan, S. and Punwani, S. (2016). “Textural analysis of multiparametric MRI detects transition zone prostate cancer”. *European Radiology*, 27(6), pp.2348-2358.

.